Hallmarks of Majorana mode leaking into a hybrid double quantum dot

Piotr Majek [1,*], Grzegorz Górski [2,†], Tadeusz Domański [3,‡] and Ireneusz Weymann [1,§]

[1]*Institute of Spintronics and Quantum Information, Faculty of Physics, A. Mickiewicz University, 61-614 Poznań, Poland*
[2]*Institute of Physics, College of Natural Sciences, University of Rzeszów, 35-310 Rzeszów, Poland*
[3]*Institute of Physics, M. Curie-Skłodowska University, 20-031 Lublin, Poland*

We investigate the spectral and transport properties of a double quantum dot laterally attached to a topological superconducting nanowire, hosting the Majorana zero-energy modes. Specifically, we consider a geometry, in which the outer quantum dot is embedded between the external normal and superconducting leads, forming a circuit. First, we derive analytical expressions for the bound states in the case of an uncorrelated system and discuss their signatures in the tunneling spectroscopy. Then, we explore the case of strongly correlated quantum dots by performing the numerical renormalization group calculations, focusing on the interplay and relationship between the leaking Majorana mode and the Kondo states on both quantum dots. Finally, we discuss feasible means to experimentally probe the in-gap quasiparticles by using the Andreev spectroscopy based on the particle-to-hole scattering mechanism.

I. INTRODUCTION

Two quantum dots contacted in various arrangements with external macroscopic reservoirs have been proposed as promising building blocks of future nanoelectronic, spintronic, and quantum information technologies [1,2]. For instance, double quantum dot (DQD) configurations provide a versatile platform for the implementation of spin-based quantum information processing systems [3]. Moreover, a rapid progress in materials science of superconducting hybrid nanostructures [4,5] stimulated vivid interest in constructing quantum bits out of the Andreev bound states [4,6–9]. Further perspectives for the realization of topological superconducting qubits are related to nanostructures involving DQDs coupled to topological superconducting wires, hosting the Majorana zero-energy modes (MZMs) at their ends, the so-called Majorana wires (MWs) [10–15]. Such platforms allow for the implementation of fault-tolerant quantum computing protocols, which are in the center of interest of quantum information research [16].

The main motivation for studying the hybrid nanostructures composed of quantum dots and Majorana wires is associated with a tendency of such end-modes to leak into the neighboring objects [17] initially predicted theoretically in Ref. [18]. Effectively, this gives rise to fractional values of the differential conductance, which serve as fingerprints of the exotic character of MZMs [19]. Various situations have been investigated so far, considering mainly single quantum dots and exploring the interplay of correlation effects with

the Majorana quasiparticles [20–28]. In this regard, much less attention has been paid to hybrid systems composed of double quantum dots hybridized with topological superconducting wires. Therefore, this work aims to shed some light on the transport properties of DQD-MW hybrid structures, focusing specifically on the setup displayed in Fig. 1.

It is important to note that the properties of double quantum dots proximitized with conventional superconductors have been studied experimentally by the tunneling spectroscopy, using InAs [5,29–32], InSb [12], Ge/Si [33], carbon nanotubes [34,35], and by the scanning tunneling microscopy (STM) applied to magnetic dimers deposited on superconducting surfaces [36–39]. In-gap bound states of the double quantum dots (dimers) have been thoroughly analyzed by a number of groups [40–57], in particular predicting quantum phase transitions, in which the total spin could vary between the singlet, doublet, and triplet states [58,59]. However, the properties of proximitized DQDs, additionally interacting with Majorana modes, are much less explored [60].

Recently, a fusion of individual bound states into their molecular (hydrogen atomlike) structure has been realized by a controllable change of the hybridization between the quantum dots contacted with superconducting reservoirs [61]. A similar process for topological bound states would be highly desirable, therefore this issue triggers intensive activities [62]. Motivated by such achievements and trends, we study the transport behavior of a hybrid double quantum dot setup, where the central quantum dot (QD_1) is embedded between the superconducting (S) and the normal metallic (N) lead (provided by, e.g., an STM tip), forming a circuit. We assume QD_1 to be connected through the second quantum dot (QD_2) to the topological superconducting nanowire, see Fig. 1. Practically, such quantum dots can be considered as being a piece of a nontopological segment of the nanowire consisting of two sites, in analogy to the experimental hybrid system

---
*pmajek@amu.edu.pl
†ggorski@ur.edu.pl
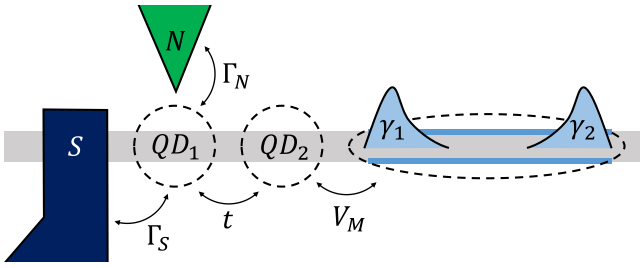‡doman@kft.umcs.lublin.pl
§weymann@amu.edu.pl

FIG. 1. Scheme of the considered hybrid structure, comprising the quantum dot (QD_1) placed between the normal (N) and superconducting (S) electrodes and side attached to the second quantum dot (QD_2) bridged with the topological superconducting nanowire, hosting Majorana end-modes described by the operators γ_1 and γ_2. An STM tip, attached to QD_1 with the coupling strength Γ_N, allows for probing the spectroscopic features of the system.

that provided the first evidence for leakage of the Majorana quasiparticles [17,25]. To obtain the most reliable predictions for the behavior of the considered system when correlations play an important role, we resort to the density-matrix numerical renormalization group (NRG) calculations [63–67]. Moreover, to provide the complete picture and deepen the understanding of transport properties of the considered DQD-MW hybrid structure, we also perform analytical calculations for an uncorrelated case.

Our study reveals that: (i) besides the conventional in-gap quasiparticle branches (originating from the hybridization of both quantum dots) there appear additional structures induced by the Majorana mode in the form of a constructive/destructive interference pattern imprinted on the spin-down/spin-up sectors of QD_1; (ii) in the Kondo regime (when the Coulomb repulsion prevails over the superconducting proximity effect) the spin-resolved spectral functions indicate the detrimental/constructive influence of the Majorana mode on $\uparrow / \downarrow$ spin sectors of QD_1. For such a strongly correlated system, we predict the optimal Andreev conductance near a crossover from the doublet to the BCS-type singlet configurations of proximitized QD_1.

The paper is organized as follows. In Sec. II we introduce the microscopic model of the studied DQD-MW system, describing our setup. Next, in Sec. III we discuss the properties of the considered hybrid structure, neglecting the Coulomb repulsion on both quantum dots. In Sec. IV we address the correlation effects in the Kondo regime, using the numerical renormalization group approach. Finally, we summarize our findings in Sec. V.

II. MODEL

In what follows, we analyze the spectroscopic and transport properties of N-QD_1-S branch (see Fig. 1), focusing on the subgap energy region. The second quantum dot QD_2 transmits the Majorana mode(s), which in turn affects the transport by interferometric effects. We study those effects in detail, considering the fully polarized case $V_{M\downarrow} = V_M$ and $V_{M\uparrow} = 0$, where $V_{M\sigma}$ is the coupling between the second dot and Majorana wire for spin σ. Some results for the arbitrary

spin-dependent couplings $V_{M\sigma}$ [25,68–70] are presented in Appendix A.

Our hybrid structure (Fig. 1) can be modeled by the following Hamiltonian:

$$H = H_N + T_N + H_{DQD} + H_{MW} + H_{SC}, \tag{1}$$

where

$$H_N = \sum_{\mathbf{k}\sigma} \varepsilon_{N\mathbf{k}} c^\dagger_{N\mathbf{k}\sigma} c_{N\mathbf{k}\sigma} \tag{2}$$

describes the metallic lead with the operators $c^\dagger_{N\mathbf{k}\sigma}$ creating electrons with spin σ, momentum $\mathbf{k}$, and energy $\varepsilon_{N\mathbf{k}}$. The second term in Eq. (1) describes the tunneling processes between the metallic lead and the first quantum dot

$$T_N = \sum_{\mathbf{k}\sigma} V_N (d^\dagger_{1\sigma} c_{N\mathbf{k}\sigma} + c^\dagger_{N\mathbf{k}\sigma} d_{1\sigma}), \tag{3}$$

where V_N is the momentum independent tunneling matrix element and $d^\dagger_{1\sigma}$ operator creates electrons with spin σ at the central quantum dot. When this quantum dot is coupled to the external contacts, it leads to the broadening of the dot level described by $\Gamma_N = \pi \rho_N V_N^2$, where V_N is assumed to be real, while ρ_N is the density of states of the metallic lead. For calculations we use the bandwidth of the metallic lead as a convenient energy unit ($D \equiv 1$).

The double quantum dot part is given by

$$H_{DQD} = \sum_{j\sigma} \varepsilon_j d^\dagger_{j\sigma} d_{j\sigma} + \sum_j U_j d^\dagger_{j\uparrow} d_{j\uparrow} d^\dagger_{j\downarrow} d_{j\downarrow}$$
$$+ \sum_\sigma t(d^\dagger_{1\sigma} d_{2\sigma} + \text{H.c.}), \tag{4}$$

where $d^\dagger_{j\sigma}$ creates a spin-σ electron on the jth quantum dot with energy ε_j. The repulsive Coulomb potential U_j between the opposite spin electrons on individual quantum dots shall be assumed equal $U_1 = U_2 = U$. These quantum dots are interconnected through the hybridization, denoted by t.

The low-energy quasiparticles of the topological nanowire can be described by the following term [71,72]:

$$H_{MW} = \sqrt{2} V_M (d^\dagger_{2\downarrow} \gamma_1 + \gamma_1 d_{2\downarrow}) + i\varepsilon_M \gamma_1 \gamma_2. \tag{5}$$

The first part couples the spin-$\downarrow$ electrons of the second quantum dot with the Majorana mode described by the operator γ_1 through the tunneling element V_M. The role of the coupling of Majorana quasiparticles to both spins of QD_2 is briefly discussed in Appendix A. The Majorana operators can be rewritten in terms of an auxiliary fermion operator f as $\gamma_1 = (f^\dagger + f)/\sqrt{2}$ and $\gamma_2 = i(f^\dagger - f)/\sqrt{2}$. In the case of a short nanowire, we should assume the overlap ε_M between the wave functions of the Majorana modes. However, here we focus on the long wire case, i.e., when the Majorana quasiparticles do not overlap and $\varepsilon_M = 0$.

The last part of the Hamiltonian (1) refers to the superconducting substrate and its coupling to QD$_1$

$$H_{SC} = \sum_{\mathbf{k}\sigma} \varepsilon_{S\mathbf{k}} c_{S\mathbf{k}\sigma}^\dagger c_{S\mathbf{k}\sigma} - \left(\Delta_{SC} \sum_{\mathbf{k}} c_{S\mathbf{k}\uparrow}^\dagger c_{S-\mathbf{k}\downarrow}^\dagger + \text{H.c.} \right)$$
$$+ \sum_{\mathbf{k}\sigma} V_S (d_{1\sigma}^\dagger c_{S\mathbf{k}\sigma} + c_{S\mathbf{k}\sigma}^\dagger d_{1\sigma}). \quad (6)$$

In the limit of large pairing gap $\Delta_{SC} \to \infty$, these terms give rise to the proximity induced on-dot pairing

$$H_{SC} \approx -\Delta_1 (d_{1\uparrow}^\dagger d_{1\downarrow}^\dagger + d_{1\downarrow} d_{1\uparrow}), \quad (7)$$

with the effective pairing potential $\Delta_1 = \Gamma_S$, and Γ_S denoting the coupling strength between QD$_1$ and the superconductor.

III. THE CASE OF THE UNCORRELATED SYSTEM

Let us start our analysis by investigating the spectral and transport properties in the case of uncorrelated quantum dots, i.e., when $U = 0$. For this purpose we use the Green's function method. The influence of the topological nanowire on the quantum dots can be captured by the matrix Green's function defined in the particle-hole (Nambu) notation $\hat{\mathcal{G}}(\omega) = \langle\langle \Psi; \Psi^\dagger \rangle\rangle_\omega$, with $\Psi = (d_{1\uparrow}, d_{1\uparrow}^\dagger, d_{1\downarrow}, d_{1\downarrow}^\dagger, d_{2\uparrow}, d_{2\uparrow}^\dagger, d_{2\downarrow}, d_{2\downarrow}^\dagger, f, f^\dagger)$. For $U = 0$, the matrix equation for the Green's function takes the following form:

$$\mathcal{G}^{-1}(\omega) = \omega \hat{I} + \begin{pmatrix} -\varepsilon_1 + i\Gamma_N & 0 & 0 & \Gamma_S & -t & 0 & 0 & 0 & 0 & 0 \\ 0 & \varepsilon_1 + i\Gamma_N & -\Gamma_S & 0 & 0 & t & 0 & 0 & 0 & 0 \\ 0 & -\Gamma_S & -\varepsilon_1 + i\Gamma_N & 0 & 0 & 0 & -t & 0 & 0 & 0 \\ \Gamma_S & 0 & 0 & \varepsilon_1 + i\Gamma_N & 0 & 0 & 0 & t & 0 & 0 \\ -t & 0 & 0 & 0 & -\varepsilon_2 & 0 & 0 & 0 & 0 & 0 \\ 0 & t & 0 & 0 & 0 & \varepsilon_2 & 0 & 0 & 0 & 0 \\ 0 & 0 & -t & 0 & 0 & 0 & -\varepsilon_2 & 0 & -V_M & -V_M \\ 0 & 0 & 0 & 0 & t & 0 & 0 & 0 & \varepsilon_2 & V_M & V_M \\ 0 & 0 & 0 & 0 & 0 & 0 & -V_M & V_M & 0 & 0 \\ 0 & 0 & 0 & 0 & 0 & 0 & -V_M & V_M & 0 & 0 \end{pmatrix}, \quad (8)$$

where $\hat{I}$ stands for the identity matrix.

A. Resonant bound states for $\Gamma_N = 0$

Consider first the conventional bound states of the proximitized double quantum dot in the absence of coupling to the Majorana nanowire [73]. In the limit of $\Gamma_N \to 0$ such in-gap resonant states are formed at

$$\varepsilon_{AD1}^\pm = \pm \frac{1}{\sqrt{2}} \sqrt{A + \sqrt{A^2 - 4B}},$$
$$\varepsilon_{AD2}^\pm = \pm \frac{1}{\sqrt{2}} \sqrt{A - \sqrt{A^2 - 4B}}, \quad (9)$$

where $A = \varepsilon_1^2 + \varepsilon_2^2 + \Gamma_S^2 + 2t^2$ and $B = (\varepsilon_1\varepsilon_2 - t^2)^2 + (\varepsilon_2\Gamma_S)^2$. The quasiparticles $\varepsilon_{AD1}^\pm$ represent the Andreev bound states of QD$_1$, $E_A^\pm = \pm\sqrt{\varepsilon_1^2 + \Gamma_S^2}$, now slightly modified by the hybridization t to QD$_2$. The other quasiparticles $\varepsilon_{AD2}^\pm$ originate from the energy level of QD$_2$ owing to the induced electron pairing (via its coupling to QD$_1$).

The attachment of the topological superconductor nanowire to the double quantum dot substantially affects the spectrum of this setup, revealing signatures of the zero-energy Majorana mode. Now, besides the initial quasiparticles $\varepsilon_{AD1}^\pm$ and $\varepsilon_{AD2}^\pm$ there emerge additional states at

$$\varepsilon_{MD1}^\pm = \pm \frac{1}{\sqrt{2}} \sqrt{A_M + \sqrt{A_M^2 - 4B_M}},$$
$$\varepsilon_{MD2}^\pm = \pm \frac{1}{\sqrt{2}} \sqrt{A_M - \sqrt{A_M^2 - 4B_M}}, \quad (10)$$

where $A_M = A + 4V_M^2$ and $B_M = B + 4V_M^2(\varepsilon_1^2 + \Gamma_S^2 + t^2)$. Let us notice that such new features depend on the coupling strength V_M. We recognize that the quasiparticle states $\varepsilon_{MD1}^\pm$ and $\varepsilon_{MD2}^\pm$ are driven by a direct coupling of the QD$_2$ and an indirect coupling of the QD$_1$ (via QD$_2$) to the Majorana mode. The quasiparticle energies $\varepsilon_{ADi}^\pm$ and $\varepsilon_{MDi}^\pm$ ($i = 1, 2$) are displayed in Figs. 2 and 3 by dashed lines.

B. Quasiparticle spectrum for $\Gamma_N \neq 0$

To discuss the empirically measurable properties of our setup (Fig. 1), let us now examine the effective spectrum for a finite (yet small) coupling Γ_N. The continuous electronic spectrum of the normal lead broadens the subgap quasiparticle states, which acquire finite lifetimes. Because the transport properties of the considered system can be related to the spectral function of the first quantum dot, in the following we shall focus on its behavior. We have computed spectral function

$$A_{i\sigma}(\omega) = -\frac{1}{\pi} \text{Im} \langle\langle d_{i\sigma}; d_{i\sigma}^\dagger \rangle\rangle_{\omega+i0^+}, \quad (11)$$

choosing such model parameters that allow for clear identification of the role played by the Majorana mode. For specific numerical calculations we use: $\Gamma_N = 0.002$, $\Gamma_S = 0.02$, $t = 0.01$, and $\varepsilon_1 = 0$ in units of bandwidth $D \equiv 1$. Figure 2 refers to the case of identical quantum dot energies $\varepsilon_1 = \varepsilon_2$, while Fig. 3 presents the case of detuned energies $\varepsilon_1 \neq \varepsilon_2$, respectively.

In the absence of topological nanowire (see the orange curves in Figs. 2 and 3), we notice two pairs of the
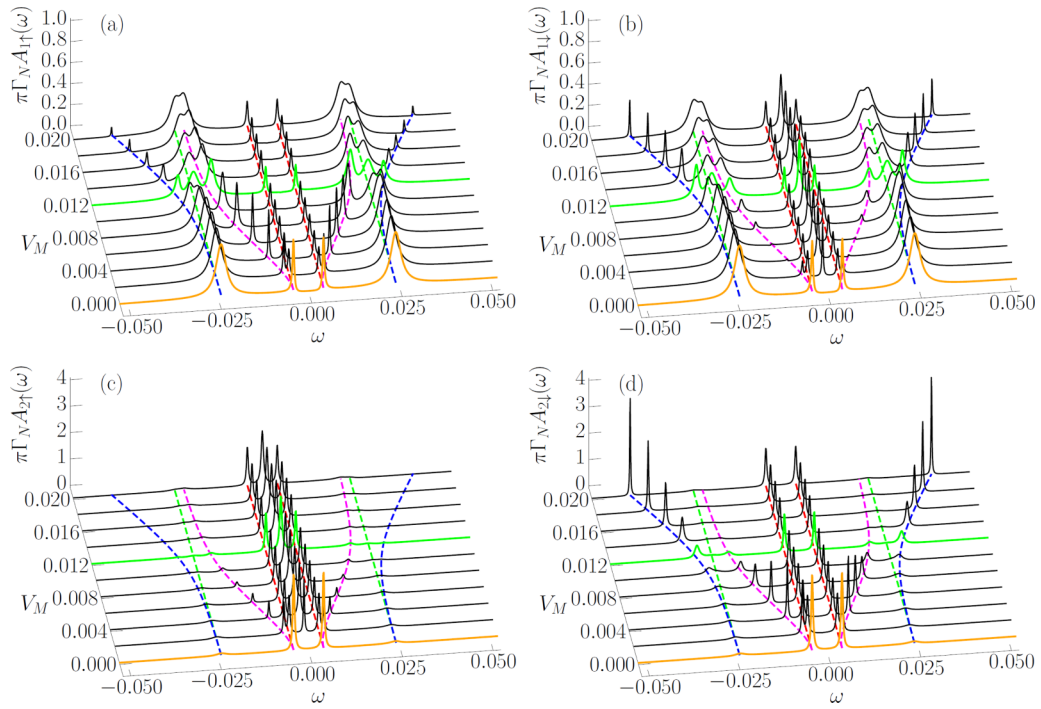
FIG. 2. The normalized spectral function $\pi\Gamma_N A_{i\sigma}(\omega)$ of QD$_1$ (a) and (b) and QD$_2$ (c) and (d) obtained for $\varepsilon_1 = \varepsilon_2 = 0$, $\Gamma_S = 0.02$, $\Gamma_N = 0.002$, and $t = 0.01$. Positions of the quasiparticle energies $\varepsilon_{ADi}^{\pm}$ and $\varepsilon_{MDi}^{\pm}$, given by Eqs. (9) and (10), are indicated by the dashed lines [$\varepsilon_{AD1}^{\pm}$ (green), $\varepsilon_{AD2}^{\pm}$ (red), $\varepsilon_{MD1}^{\pm}$ (blue), and $\varepsilon_{MD2}^{\pm}$ (magenta)]. All energies are expressed in units of the bandwidth ($D \equiv 1$).

Andreev peaks centered at $\varepsilon_{AD1}^{\pm}$ and $\varepsilon_{AD2}^{\pm}$ accompanied by the interferometric (Fano-type) structure at $\omega = \varepsilon_2$. The direct coupling of QD$_2$ to the topological nanowire indirectly affects the electronic states of QD$_1$. Such influence is transmitted via

spin-$\downarrow$ electrons of the second quantum dot. In consequence, the leakage of Majorana mode shows up at zero energy of the spin-down spectral function $A_{1\downarrow}(\omega)$. For $\varepsilon_1 = \varepsilon_2$ and arbitrary couplings $V_M \neq 0$, we obtain the universal values
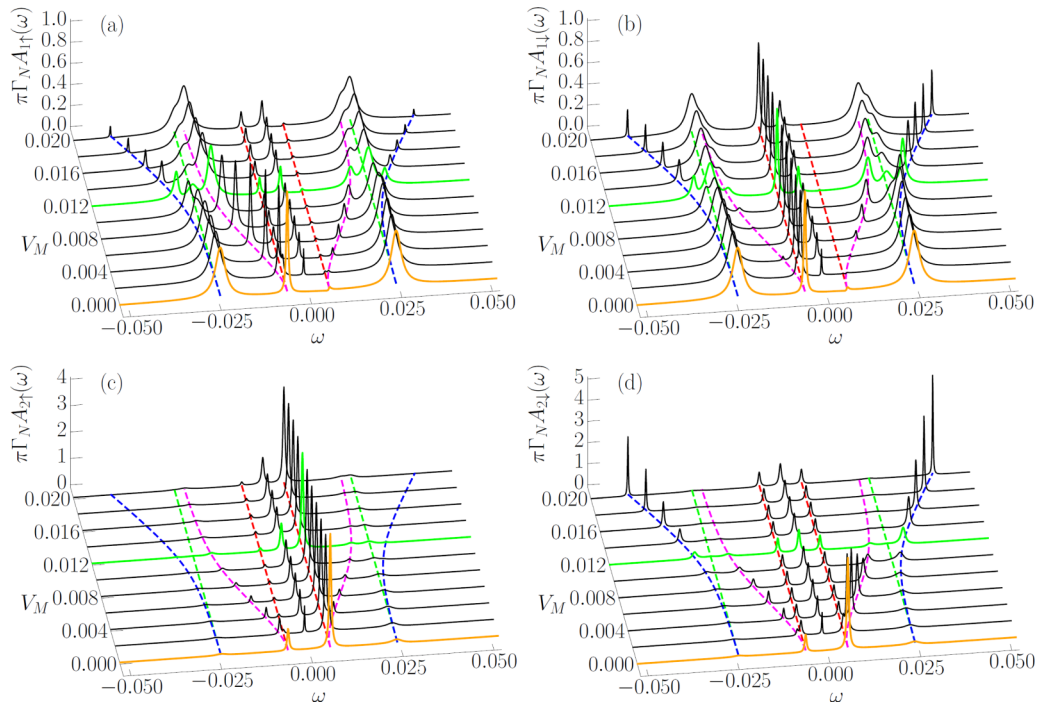

FIG. 3. Spectral functions $\pi\Gamma_N A_{i\sigma}(\omega)$ obtained for finite detuning of the energy levels $\varepsilon_1 = 0$ and $\varepsilon_2 = 0.005$, using the same model parameters as in Fig. 2.

$A_{1\downarrow}(0) = 1/2\pi\Gamma_N$ and $A_{1\uparrow}(0) = 0$, see Fig. 2, in analogy to the previously reported behavior of single dot configurations [26].

The coupling V_M is responsible for additional features, appearing at $\varepsilon_{MD1}^{\pm}$ and $\varepsilon_{MD2}^{\pm}$, whereas the quasiparticle states $\varepsilon_{AD1}^{\pm}$ and $\varepsilon_{AD2}^{\pm}$ practically do not change their energies (see green and red dashed lines), except for their spectral weights. For the weak coupling V_M, the quasiparticle states $\varepsilon_{MD1}^{\pm}$ co-incide with $\varepsilon_{AD1}^{\pm}$, while the other states $\varepsilon_{MD2}^{\pm}$ are pushed to higher energies. On the other hand, for stronger couplings V_M, we observe the development of a molecular structure, in which $\varepsilon_{MD2}^{\pm}$ are mixed with $\varepsilon_{AD1}^{\pm}$. Figures 2 and 3 show that the quasiparticles $\varepsilon_{MD1}^{\pm}$ have the dominant spectral weights in the spin-$\downarrow$ sector, whereas the states $\varepsilon_{MD2}^{\pm}$ gain their spectral weights mainly in the spin-$\uparrow$ sector.

Let us now inspect the role of QD$_2$ detuning from the particle-hole symmetry point ($\varepsilon_2 \neq 0$). Under such conditions, the Majorana peak is observable in both spin components of the spectral function $A_{1\sigma}(\omega)$, see Fig. 3. The width of the zero-energy peak depends on the coupling V_M, while the height ratio $A_{1\downarrow}(0)/A_{1\uparrow}(0)$ is controlled by the energy level ε_2, keeping the total spectral function $A_{1\uparrow}(0) + A_{1\downarrow}(0) \approx 1/2\pi\Gamma_N$. For the case of strong coupling V_M, we obtain $A_{1\uparrow}(0) > A_{1\downarrow}(0)$, and additionally there emerges a Fano-type dip in $A_{1\uparrow}(\omega)$ at $\omega = \varepsilon_2$. Such an interferometric feature is absent in $A_{1\downarrow}(\omega)$ because of the hybridization of spin-$\downarrow$ electrons of the second quantum dot with the Majorana nanowire.

The second quantum dot (QD$_2$) is indirectly affected by the superconducting reservoir, absorbing the electron pairing [73–77]. Figure 4 shows the variation of the pairing correlations $\langle d_{i\downarrow} d_{i\uparrow} \rangle$ induced on the first ($i = 1$) and the second ($i = 2$) quantum dot with respect to the coupling V_M for several values of the energy level of QD$_2$. For $\varepsilon_2 = 0$ and $V_M = 0$ we reproduce the standard result $\langle d_{1\downarrow} d_{1\uparrow} \rangle = \langle d_{2\downarrow} d_{2\uparrow} \rangle$ reported in Ref. [74]. Upon detuning the quantum dot energy levels, we observe that pairing correlations of QD$_2$ are gradually suppressed, at an expense of enhancing the effective pairing on the central quantum dot (QD$_1$). The coupling of QD$_2$ to Majorana nanowire has a rather minor influence on all pairing sectors, it merely weakens the pairing correlations $\langle d_{2\downarrow} d_{2\uparrow} \rangle$ on the second quantum dot.

In Appendix B we provide more specific evidence for the Majorana-type features transmitted from the topological nanowire to each spin sector of the quantum dots, using the procedure introduced in Refs. [10,18]. In particular, for identical energy levels ($\varepsilon_1 = \varepsilon_2 = 0$), we observe the leakage of the Majorana zero-energy mode solely to the spin-$\uparrow$ of the inner QD$_2$ and spin-$\downarrow$ of the outer QD$_1$. The opposite spin sectors do not absorb the Majorana zero-energy mode, because of the interferometric effects. Such a situation is no longer present for the detuned energy levels $\varepsilon_1 \neq \varepsilon_2$.

C. Linear Andreev conductance

The Majorana mode features leaking into the quantum dots could be detected by the charge transport measurements [17,78–81]. In our setup, the central quantum dot (QD$_1$) is embedded between the normal and superconducting electrodes, so its subgap states should be observable in the Andreev current measurements [82–85]. From the theoretical side, the
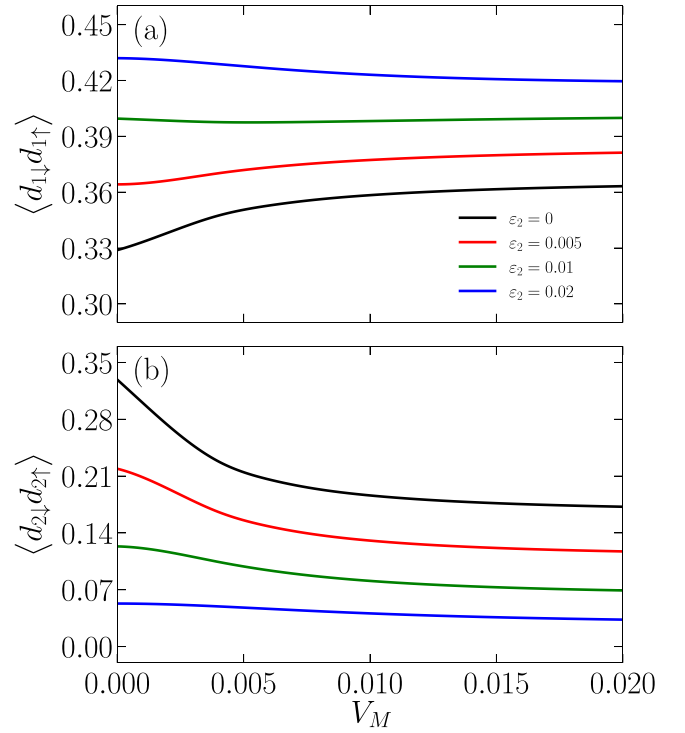

FIG. 4. The proximity induced pairing on (a) the first (QD$_1$) and (b) the second (QD$_2$) quantum dot as a function of the coupling V_M to the Majorana wire obtained for $\varepsilon_1 = 0$ and several values of ε_2, as indicated. The other parameters are the same as in Fig. 2.

Andreev current can be calculated from

$$I_A(V) = \frac{e}{h} \int d\omega \, T_A(\omega)[f(\omega - eV) - f(\omega + eV)], \quad (12)$$

where $f(x) = [1 + \exp(x/k_B T)]^{-1}$ denotes the Fermi-Dirac distribution function and the energy-dependent Andreev transmittance is given by

$$T_A(\omega) = \Gamma_N^2 \sum_\sigma |\langle\langle d_{1\sigma}; d_{1\bar{\sigma}} \rangle\rangle_{\omega + i0^+}|^2. \quad (13)$$

For $t = 0$, the optimal value of the low-temperature Andreev conductance $G_A(V) = dI_A(V)/dV$ is $4e^2/h$ [82,86–88]. Finite hopping between the dots, however, lowers this maximum value. Moreover, the side-attached Majorana nanowire can result in a further reduction of the Andreev conductance down to e^2/h [26,89,90].

In what follows, we briefly investigate the influence of the Majorana mode on the Andreev conductance measured in the N-QD$_1$-S circuit. Figure 5 presents the linear (zero-bias) Andreev conductance G_A as a function of ε_2 calculated for a fixed value of the first dot level position $\varepsilon_1 = 0$. It can be seen that in the absence of coupling to the Majorana mode, the Andreev conductance is relatively low, see the solid curve in Fig. 5(a). However, once V_M is finite, we observe an enhancement of the Andreev conductance to $G_A = G_A^{\max}/4$ at some nonzero value of ε_2, with $G_A^{\max} = 4e^2/h$ the maximum Andreev conductance. Such value of G_A reflects the fractional nature of the Majorana mode leaking to the DQD. In fact, the enhancement of Andreev conductance from 0 to e^2/h with detuning the second dot level may serve as a signature of the
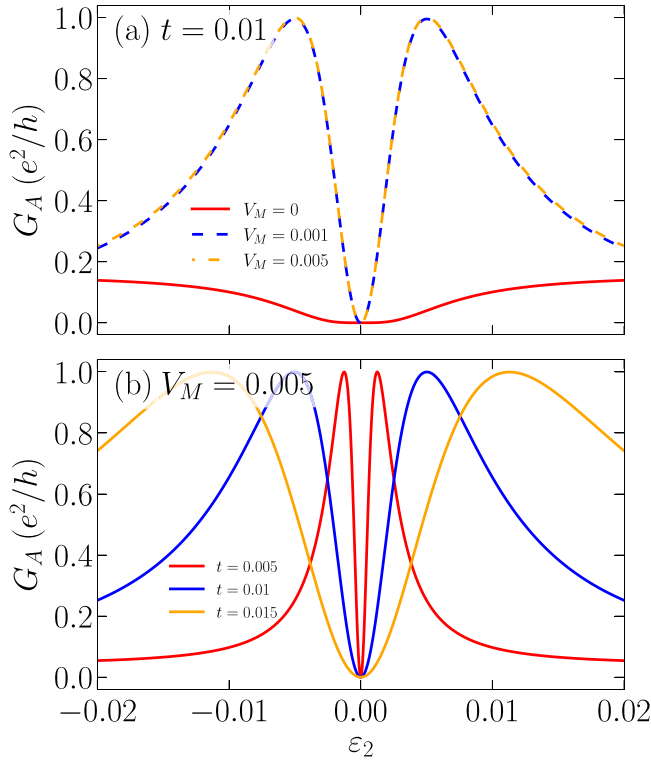
FIG. 5. The linear (zero-bias) Andreev conductance $G_A = \frac{dI_A(V)}{dV}|_{V=0}$ in units of e^2/h as a function of the energy level ε_2 obtained for (a) several values of the coupling V_M, assuming $t = 0.01$, and (b) for different interdot couplings t, assuming $V_M = 0.005$. The other parameters are the same as in Fig. 2.

MZM in the system. We also note that the Andreev conductance exhibits a perfect vanishing that occurs for $\varepsilon_1 = \varepsilon_2 = 0$, caused by destructive Fano-type interference, which is robust against any other phenomena. For a given interdot coupling t, the linear Andreev conductance rather weakly depends on the coupling V_M [see Fig. 5(a)]. However, for a fixed value of coupling V_M, G_A is very sensitive to interdot hybridization t [see Fig. 5(b)]. In the weak interdot hopping limit, the conductance G_A achieves its optimal value at small values of the second quantum dot energy level ε_2. On the other hand, when the interdot coupling becomes stronger, the position of the energy level ε_2, at which the Andreev conductance is optimal, substantially increases.

The linear Andreev conductance is also dependent on the first quantum dot energy level. This situation is shown in Fig. 6, which displays the Andreev conductance as a function of both quantum dot energy levels for three selected values of t and V_M. As can be seen, no matter what the value of ε_1 is, G_A always vanishes for $\varepsilon_2 = 0$. This characteristic feature is caused by the destructive quantum interference. Figure 6 displays the typical Fano line shape of such entirely suppressed linear conductance of the considered setup.

IV. THE CASE OF THE KONDO REGIME

We now address the situation when the Coulomb correlations in the quantum dots are relevant, $U \neq 0$. In this case new effects emerge that are exclusively due to electron
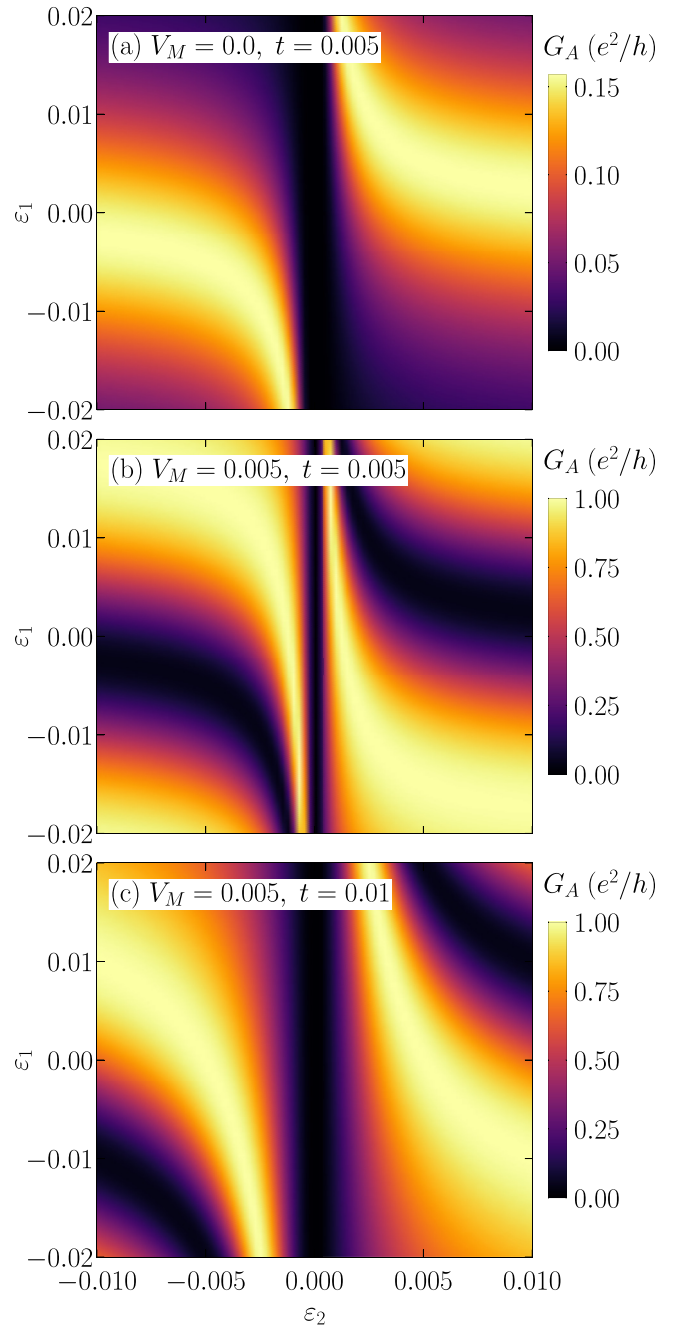

FIG. 6. The linear Andreev conductance G_A as a function of the first and second quantum dot energy levels calculated for (a) $V_M = 0$, $t = 0.005$, (b) $V_M = 0.005$, $t = 0.005$, and (c) $V_M = 0.005$, $t = 0.01$.

correlations. One of these effects is the Kondo phenomenon [91], in which a correlated state is formed between the quantum dots and the conduction band electrons of the normal lead [92]. The main goal of this section is to examine the system's transport properties in the Kondo regime, and to shed light on the interplay of Kondo correlations, electron pairing, and Majorana modes.

In the large pairing gap limit of the superconductor, the Kondo effect can be induced by the spin-exchange coupling between QD_1 and the metallic lead [93]. Efficiency of such

interaction is sensitive to the competition between the on-dot pairing and the Coulomb repulsion. The Kondo state would arise if QD_1 is in the singly occupied configuration $|\sigma\rangle$, which takes place when the Coulomb repulsion dominates over the superconducting proximity effect $\Gamma_S < U/2$. Furthermore, the magnitude of the exchange interaction is substantially enhanced near a transition between the spinful $|\sigma\rangle$ and the spinless (BCS type) $u|0\rangle - v|\uparrow\downarrow\rangle$ configurations [94,95]. Since this parity change of QD_1 is manifested by a crossing of the in-gap bound states, therefore the influence of the zero-energy Majorana mode on this crossing would be very important.

The relationship between the subgap Kondo effect and the Majorana physics has been previously investigated in heterostructures with a single correlated quantum dot [26,90]. Here we extend these studies to the double quantum dot system (Fig. 1), where the Majorana mode can affect QD_1 only indirectly, via the second quantum dot. For efficiency of this two-stage Majorana leakage, one should also take into account the Kondo effect developed in QD_2 [15,96,97]. With lowering the energy scale below the Kondo temperature T_K, the Kondo effect first develops in the first quantum dot, giving rise to enhanced conductance [98]. However, for even lower energies, the spin on the second quantum dot becomes screened and, because this dot is not directly coupled to the superconductor-normal lead circuit, cf. Fig. 1, the conductance becomes in turn suppressed. This is known as the two-stage Kondo effect, which is characterized by a dip in the spectral function of width proportional to the second-stage Kondo temperature T^* [99–102]. In what follows, we analyze a subtle interplay of these effects and discuss their signatures observable in the charge transport properties of the N-QD_1-S circuit.

To reliably treat the low and high energy features originating from the correlation effects and the proximity-induced pairing, we perform the density-matrix numerical renormalization group calculations [63–67]. We impose the band discretization parameter $\Lambda = 2$–2.2, keeping at least 2000 states during the iterative diagonalization. The microscopic model (1) satisfies the $Z(2)$ parity, which we implement to facilitate the numerical calculations. We perform the computations for the particle-hole symmetric case $\varepsilon_1 = \varepsilon_2 = -U/2$, assuming $U/D = 0.1$, $\Gamma_N/D = 0.01$.

A. Superconducting pairing correlations

Before analyzing the spectral and transport properties of the system, let us examine the superconducting pairing correlations induced in both quantum dots. These correlations are presented in Fig. 7 versus the coupling to superconductor Γ_S for selected values of the coupling to Majorana wire V_M. First of all, we note that the correlations ($U > 0$) strongly modify $\langle d_{i\downarrow}d_{i\uparrow}\rangle$ in comparison to the uncorrelated case, cf. Figs. 4 and 7. The induced pairing $\langle d_{1\downarrow}d_{1\uparrow}\rangle$ resembles properties typical for the single correlated quantum dot proximitized to the superconductor [93,95]; it is suppressed in the doublet state, for $\Gamma_S < U/2$, and $\langle d_{1\downarrow}d_{1\uparrow}\rangle \approx 1/2$ on the BCS singlet side, for $\Gamma_S > U/2$. Moreover, we find that in the strongly correlated case $\langle d_{1\downarrow}d_{1\uparrow}\rangle$ rather weakly depends on V_M, see Fig. 7(a). This is in contrast to the behavior of $\langle d_{2\downarrow}d_{2\uparrow}\rangle$, which is substantially enhanced by the Majorana wire, see Fig. 7(b).
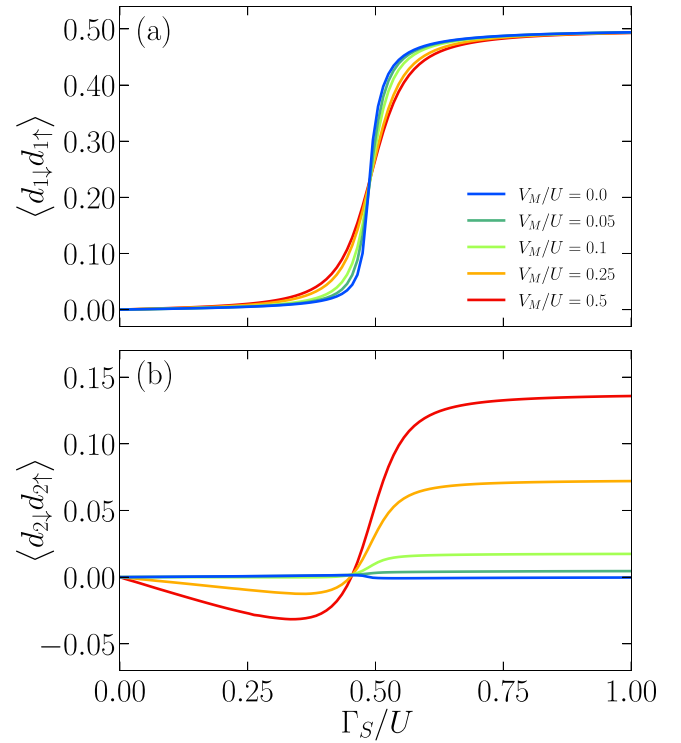

FIG. 7. Superconducting pairing correlations of (a) the first and (b) the second quantum dot calculated as a function of the coupling to superconductor Γ_S for different values of V_M, as indicated. The other parameters are: $t/U = 0.025$, $\Gamma_N/U = 0.1$, $\varepsilon_1 = \varepsilon_2 = -U/2$, and $U = 0.1$ in units of bandwidth.

Variation of $\langle d_{2\downarrow}d_{2\uparrow}\rangle$ with respect to Γ_S and V_M is much more subtle. For $\Gamma_S < U/2$, it is negative, whereas for $\Gamma_S > U/2$, it becomes positive and increases in absolute value.

We assign the qualitative and quantitative changes of the electron pairing $\langle d_{i\downarrow}d_{i\uparrow}\rangle$ observed around $\Gamma_S = U/2$ to the parity crossings. To clarify it, let us recall the well studied case of the Anderson impurity coupled to superconductor ($t = 0 = V_M$). It has been firmly established [93] that for $\Gamma_S < U/2$ the ground state of QD_1 is characterized by the singly occupied configuration $|\sigma\rangle$ (which is doubly degenerate in the absence of magnetic field), whereas for $\Gamma_S > U/2$ it takes the BCS form $|BCS\rangle = u|0\rangle + v|\uparrow\downarrow\rangle$ with appropriate coefficients u and v [93]. This fact explains an abrupt increase of $\langle d_{1\downarrow}d_{1\uparrow}\rangle$ displayed in Fig. 7(a) upon traversing the critical coupling $\Gamma_S = U/2$. We furthermore notice that neither the second quantum dot nor the topological nanowire have meaningful influence on this doublet-singlet transition of QD_1.

As regards the electron pairing of QD_2 the situation is different because it is not directly coupled to the superconducting lead. Residual value of $\langle d_{2\downarrow}d_{2\uparrow}\rangle$ presented in Fig. 7(b) by the blue line (corresponding to $V_M = 0$) indicates that a major contribution to the electron pairing of QD_2 comes from the topological superconductor. In fact, upon increasing the coupling V_M the absolute value $|\langle d_{2\downarrow}d_{2\uparrow}\rangle|$ is amplified for all couplings Γ_S. At the critical coupling $\Gamma_S = U/2$ we notice the sign reversal of $\langle d_{2\downarrow}d_{2\uparrow}\rangle$. This π shift is associated with the parity change of QD_1, or strictly speaking its feedback on QD_2.
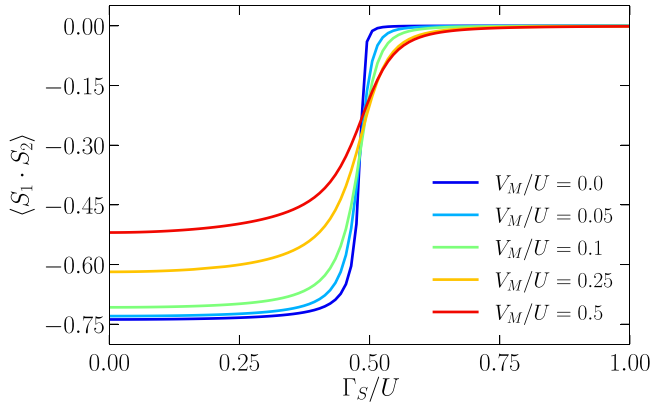
FIG. 8. Spin-spin correlation function $\langle \mathbf{S}_1 \cdot \mathbf{S}_2 \rangle$ as a function of Γ_S/U obtained for several values of V_M, using the same set of model parameters as in Fig. 7.

Since we are considering the regime of strongly coupled quantum dots, there could be expected a tendency toward a local singlet formation. Whether this mechanism does really occur or not, would strongly depend on Γ_S/U. In particular, for $\Gamma_S/U > 0.5$, the outer quantum dot (QD$_1$) is in the spinless BCS-type configuration therefore any spin locking is impossible. In the opposite limit ($\Gamma_S/U < 0.5$), however, the quantum dots indeed lock their spins, see Fig. 8. This resembles the behavior of two correlated quantum dots confined in the Josephson junction reported in Ref. [50].

In our setup (Fig. 1) we notice a detrimental influence of the Majorana mode on such spin locking for $\Gamma_S/U < 0.5$. We assign this effect to partial depletion of the low-energy spectral functions of QD$_1$ indirectly caused by the Majorana mode. This issue is analyzed in Sec. IV B.

B. Majorana features in spectral functions

To elucidate the role of the Majorana mode on the spectral density, we first analyze the dependence of the spectral function of the half-filled quantum dots on the strength of coupling to the superconductor in the absence of coupling to Majorana wire. The normalized spectral function for spin σ (note that for $V_M = 0$ the spin degeneracy is restored) is presented in Fig. 9. Let us recall that in the absence of the interdot coupling ($t = 0$) the parity change of QD$_1$ from $|\sigma\rangle$ to $u|0\rangle - v|\uparrow\downarrow\rangle$ configuration occurs at $\Gamma_S = U/2$. The subgap Kondo effect can thus be realized for $\Gamma_S < U/2$. On the other hand, for finite t but $\Gamma_S = 0$, one observes the behavior typical for the two-stage Kondo effect [100–102], with suppressed spectral density for $\omega < T^*$. In the case of finite t and Γ_S, the interplay of the on-dot pairing and Kondo correlations gives rise to an interesting behavior of the spectral function. The proximity induced pairing affects $A_{1\sigma}(\omega)$ by lifting the second stage of screening and giving rise to a finite value of $A_{1\sigma}(0)$, which is the largest around the transition between the doublet and BCS singlet state, $\Gamma_S \approx U/2$, see Fig. 9.

Let us now examine the behavior of the spectral functions in the case of finite coupling to topological nanowire, focusing on values of Γ_S around the singlet-doublet transition, cf. the dashed lines in Fig. 9. The corresponding spin-resolved spectral functions $A_{1\sigma}(\omega)$ obtained for various couplings V_M to the
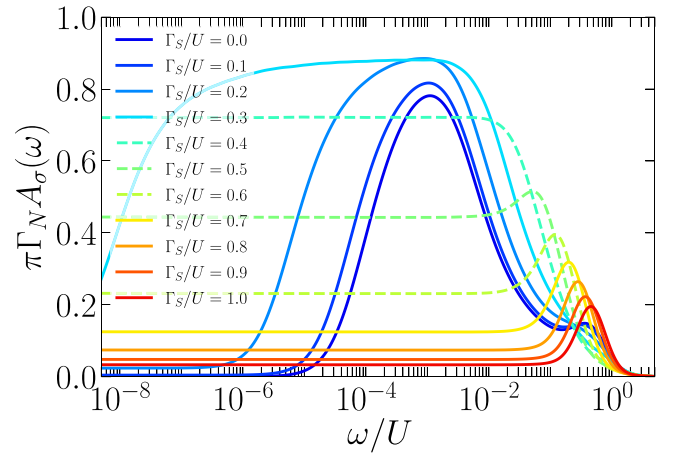

FIG. 9. The normalized spectral function $\pi\Gamma_N A_{1\sigma}(\omega)$ of the half-filled central quantum dot obtained for various couplings to superconductor Γ_S, as indicated, while $V_M = 0$. The other parameters are the same as in Fig. 7. The spectral function is symmetric with respect to the Fermi energy, therefore only positive energies are shown. Note also the logarithmic energy scale. The dashed curves correspond to the values of Γ_S analyzed in Figs. 10 and 11.

topological nanowire are presented in Figs. 10 and 11. First of all, we note that the numerical results reveal qualitative differences between the spectra of the spin-up and spin-down electrons, which should be attributed to the presence of Majorana mode. Such influence is predominantly manifested in the low-energy sector, therefore our plots are presented in a logarithmic scale. The upper panels of the figures correspond to the situation when $\Gamma_S < U/2$ and the subgap Kondo effect can be realized, therefore $A_\sigma(\omega)$ has a relatively large weight at the Fermi energy for $V_M = 0$. On the other hand, the lower panels display the case of $\Gamma_S > U/2$, where the weight is much reduced. However, once V_M is finite, these features may be completely changed.

Consider first the case of the spin-up spectrum of QD$_1$ shown in Fig. 10. Each panel of the figure clearly displays a substantial depletion of the low-energy states driven by the Majorana mode. In the weak coupling limit, $V_M \ll U$, such destructive influence appears in the form of an interferometric dip formed on top of either the subgap Kondo peak [in the strongly correlated limit $\Gamma_S/U = 0.4$, see Fig. 10(a)], or on a flat background between the Andreev peaks [corresponding to the BCS-type configuration $\Gamma_S/U = 0.6$, see Fig. 10(c)]. Upon increasing the coupling V_M, we observe the development of a molecular structure, where the Kondo effect gets suppressed. In other words, in the subgap Kondo regime, one can see a supporting influence of the coupling to the Majorana mode on the second-stage Kondo effect, i.e., there occurs a restoration of this effect for finite V_M. Moreover, the stronger the coupling V_M is, the higher the second-stage Kondo temperature T^* becomes. This picture resembles itself through the singlet-doublet transition, lowering the maximum of the Kondo peak, and finally suppressing the spectral function in the BCS regime, where the Kondo effect does not develop. Thus, the coupling to the topological nanowire has a rather destructive influence on the low-energy behavior of the spin-up spectral function.
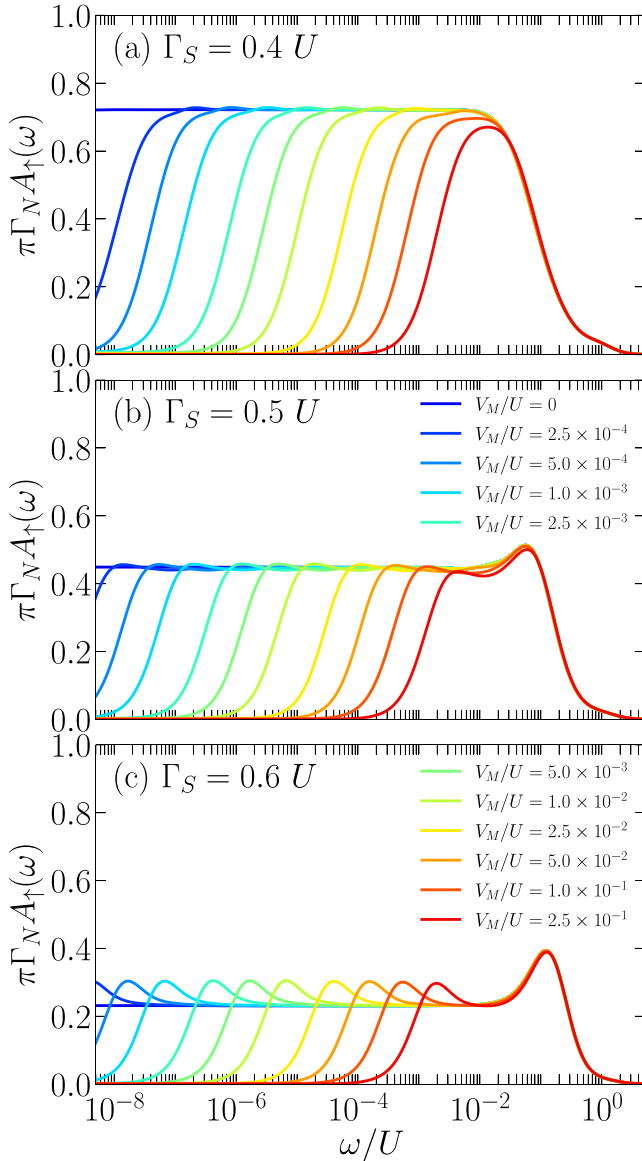
FIG. 10. The normalized spin-up spectral function $\pi\Gamma_N A_{1\uparrow}(\omega)$ calculated for different couplings V_M to the topological wire, as indicated. The top, middle, and bottom panels refer to $\Gamma_S/U = 0.4$, 0.5, and 0.6, respectively. The other parameters are the same as in Fig. 7.

In contrast to this tendency, the Majorana mode has a more complex impact on the spin-down spectral function shown in Fig. 11. In the subgap Kondo regime, finite coupling to the topological superconductor suppresses the low-energy spectral density by around $1/3$ to the universal value of $A_{1\downarrow}(0) = 1/2\pi\Gamma_N$. However, the picture changes when the BCS configuration is formed and the influence of V_M becomes constructive. For weak couplings, $V_M \ll U$, we notice a buildup of the narrow peak at zero energy due to the leaking Majorana mode. Upon increasing V_M, the value of the spectral function $A_{1\downarrow}(0)$ saturates, while the zero-energy peak gradually broadens. For larger values of V_M, this zero-energy quasiparticle state dominates over all other subgap features. The corresponding spectral function develops then its
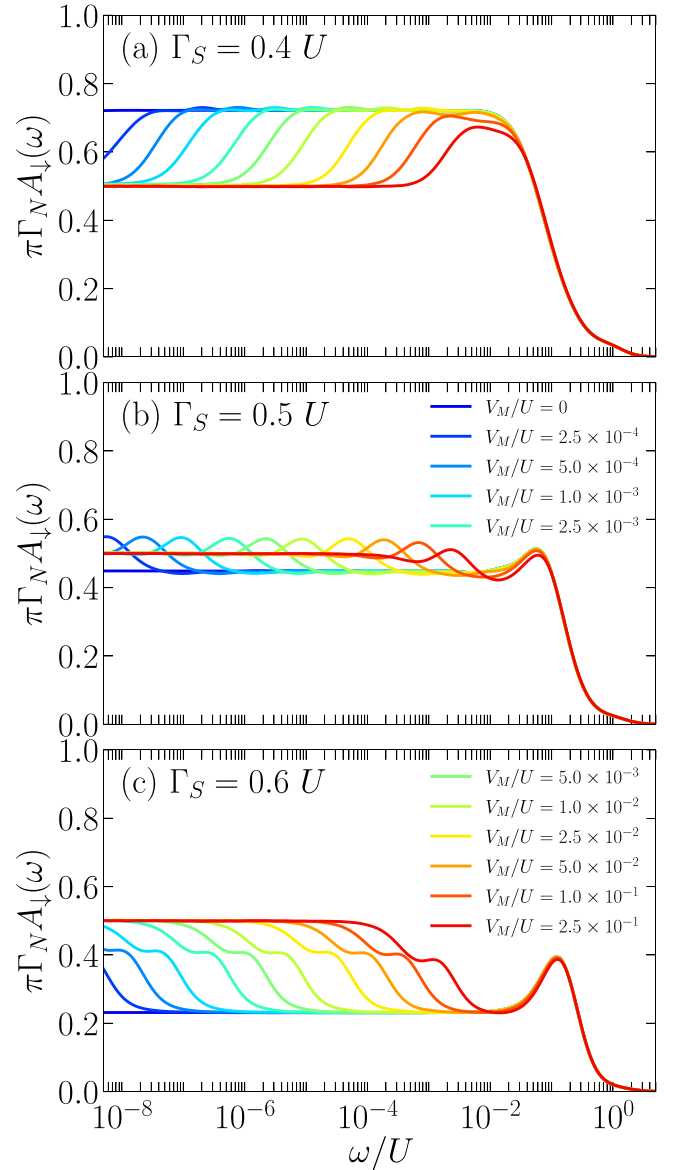
FIG. 11. The normalized spectral function for the spin-down electrons $\pi\Gamma_N A_{1\downarrow}(\omega)$ calculated for the same model parameters as in Fig. 10.

universal shape with the characteristic value $A_{1\downarrow}(0) = 1/2\pi\Gamma_N$, regardless of the Coulomb potential U. Summarizing, the attachment of the topological superconductor to the spin-$\downarrow$ electrons of QD_2 induces the zero-energy state in the spin-$\downarrow$ sector of QD_1 with the fractional value of the low-energy spectral function.

C. Subgap charge transport

Empirical detection of the quasiparticle spectra of QD_1 can be done with the use of the charge tunneling spectroscopy. In the subgap region the only transport channel is contributed by the particle-to-hole (Andreev) scattering mechanism, which combines both spin components. The subgap tunneling spectroscopy would hence provide important information about the convoluted spin-up and spin-down spectra.
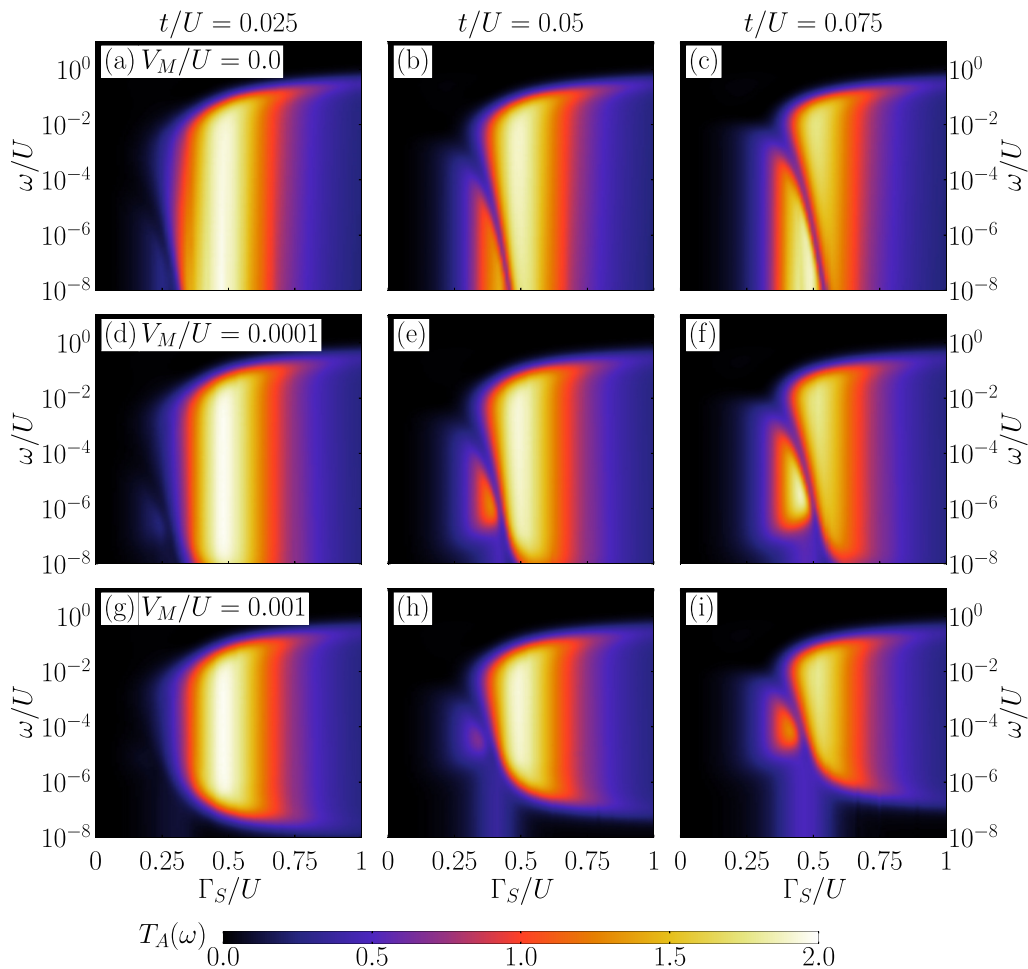
FIG. 12. The Andreev transmittance $T_A(\omega)$ as a function of Γ_S/U and energy ω calculated for several values of the coupling to Majorana wire V_M and interdot hopping t (as indicated) obtained by NRG. The other parameters are the same as in Fig. 7.

At low temperatures the Andreev differential conductance $G_A(V) = dI_A(V)/dV$ can be approximated by the Andreev transmittance $T_A(\omega)$ taken at $\omega = eV$, $\lim_{T \to 0} G_A(V) = \frac{2e^2}{h} T_A(\omega = eV)$. We display $T_A(\omega)$ in Fig. 12 for several values of the interdot hopping t (panels from left to right) and different couplings V_M (panels from top to bottom). In general, we notice that the Andreev conductance achieves its optimal value $4e^2/h$ near $\Gamma_S \approx U/2$ [88]. This situation corresponds to the ground state changeover of QD_1, whose in-gap bound states tend to cross each other and simultaneously the subgap Kondo peak is enhanced (on the doublet side).

As regards the Majorana mode, its influence shows up by suppression of the zero-bias conductance (see the middle and bottom panels in Fig. 12). This effect comes merely from the destructive quantum interference of the Majorana mode on the spin-↑ sector of QD_1 spectrum. Additionally, upon increasing the interdot hopping t, we observe the signatures of emerging molecular bound states. In particular, this is visible by a dark region splitting the optimal conductance. We note that for a more precise and direct observability of all the spin-resolved spectra of QD_1 one could use the spin-polarized Andreev spectroscopy of bound states [103].

V. SUMMARY

We have studied the influence of the Majorana mode transmitted to the double quantum dot side attached to a topological superconducting nanowire. This setup could be probed by tunneling spectroscopy through a circuit with the outer quantum dot (QD_1) sandwiched between the normal and superconducting leads. Proximity of DQD to the superconducting reservoir induces the in-gap bound states, whose complex structure depends on the interdot coupling, as recently revealed in Ref. [61]. Here we have inspected the modification of these conventional bound states by the topological superconducting nanowire hosting the Majorana boundary mode. This issue might be important for designing the braiding protocols of Majorana quasiparticles.

In the absence of correlation effects we have derived analytical expressions for the resulting in-gap bound states, identifying the trivial Andreev quasiparticle branches and the additional structures induced by the Majorana mode. We have shown that these features manifest themselves differently in each spin sector. In particular, the zero-energy quasiparticle state induced at QD_1 appears in a form of destructive/constructive interference pattern imprinted on the

↑ / ↓ spin sectors. Since the subgap charge transport mixes both spins through the particle-to-hole scattering, the resulting tunneling characteristics are predominantly affected by these destructive signatures. We have discussed them in detail, considering the linear subgap Andreev conductance.

We have also extended our considerations to the strongly correlated nanostructure, treating the competition of the superconducting proximity effect with the repulsive Coulomb interactions by the numerical renormalization group technique. Focusing on the half-filled quantum dots, we have studied both the Kondo regime, when the Coulomb repulsion dominates over the superconducting proximity effect, as well as the opposite limit, where the superconducting proximity-induced pairing surpasses the Kondo correlations. We have revealed qualitative differences in these two regimes, evidenced in the spin-resolved spectral functions. We have predicted that the optimal Andreev conductance would occur near a crossover between the singly occupied doublet to the BCS-type configurations of QD_1. Moreover, our numerical results obtained for the subgap spectroscopy indicate that the Majorona mode strongly suppresses the zero-bias conductance, owing to its destructive influence on spin-↑ sector of the outer quantum dot. We recently noticed similar studies of the Majorana modes leaking to two quantum dots embedded at opposite sides of the topological superconducting nanowire that have revealed noticeable influence of the Coulomb repulsion [104].

APPENDIX A: ROLE OF POLARIZATION

In this Appendix we extend the discussion of the properties of our hybrid structure in the uncorrelated case by assuming that both spins of QD_2 are coupled to the Majorana nanowire though with different amplitudes $V_{M\sigma}$. Hoffman *et al.* [68] have shown that the spin-dependent tunneling amplitudes between Majorana modes and the quantum dot depend on the quantum dot distance to the topological section. Moreover, such finite polarization of the quantum dot attached to the topological nanowire has been proposed as a suitable tool for probing the topology of Majorana wave function [25,68–70]. To account for this effect, we use the following parametrization of the spin-dependent amplitudes

$$V_{M\uparrow} = V_M \sin\left(\frac{\theta}{2}\right), \tag{A1}$$

$$V_{M\downarrow} = V_M \cos\left(\frac{\theta}{2}\right), \tag{A2}$$

in terms of the canting angle θ [69], corresponding to the rotation around the *y* axis.

Figure 13 presents the variation of the spectral function $A_{1\sigma}(\omega)$ of each spin sector with respect to the canting angle θ. One can clearly see the influence of θ on spectral
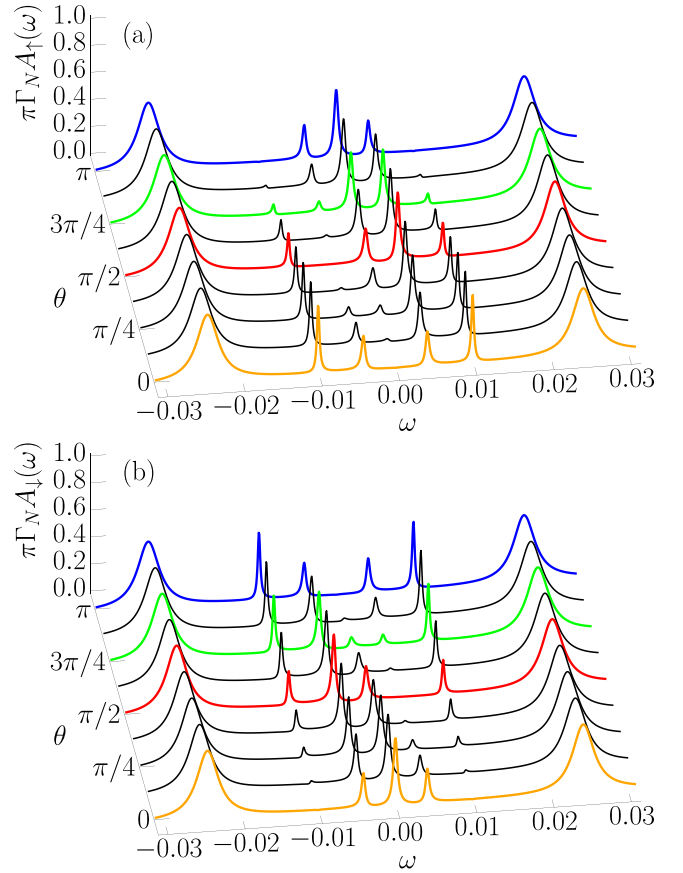

FIG. 13. The normalized spectral function $\pi\Gamma_N A_{1\sigma}(\omega)$ for (a) the spin-up and (b) spin-down components as a function of the canting angle θ. Results are obtained for the case of uncorrelated quantum dots using the following model parameters: $\varepsilon_1 = \varepsilon_2 = 0$, $V_M = 0.005$, $t = 0.01$, $\Gamma_S = 0.02$, $\Gamma_N = 0.002$.

weights of the zero-energy peak, and also on the finite-energy quasiparticles. In the fully polarized cases, $V_{M\uparrow} = 0$ and $V_{M\downarrow} = V_M$ ($V_{M\uparrow} = V_M$ and $V_{M\downarrow} = 0$), corresponding to $\theta = 0$ ($\theta = \pi$), we obtain the Majorana peak of spin-↓ (spin-↑) spectral function $A_{1\downarrow}(0) = 1/2\pi\Gamma_N$ [$A_{1\uparrow}(0) = 1/2\pi\Gamma_N$]. On the other hand, in the unpolarized case, i.e., $\theta = \frac{\pi}{2}$, the zero-energy Majorana peak is identical in both spin sectors, $A_{1\uparrow}(0) = A_{1\downarrow}(0) = 1/4\pi\Gamma_N$. Additionally, we notice, that the canting angle neither affects the energies of the Andreev bound states $\varepsilon_{ADi}^\pm$ [cf. Eq. (9)] nor the quasiparticle states $\varepsilon_{MDi}^\pm$ [cf. Eq. (10)]. Its influence is visible merely in the spectral densities $A_{1\sigma}(\varepsilon_{AD2}^\pm)$ and $A_{1\sigma}(\varepsilon_{MDi}^\pm)$.

We have shown that θ affects the quasiparticle weights of the diagonal spectral functions, but additionally it also strongly modifies the off-diagonal spectral functions. Such influence would be empirically observable in the subgap tunneling conductance. Figure 14 presents the linear Andreev conductance G_A as a function of the canting angle. We notice that θ leads to the variation of G_A up to the maximal value $G_A^{\max} = e^2/h$. For the full polarization of $V_{M\sigma}$ (i.e., $\theta = 0$ or $\theta = \pi$), we obtain identical values of the linear conductance, because then the particle and hole degrees of freedom equally participate in the Andreev scattering mechanism.
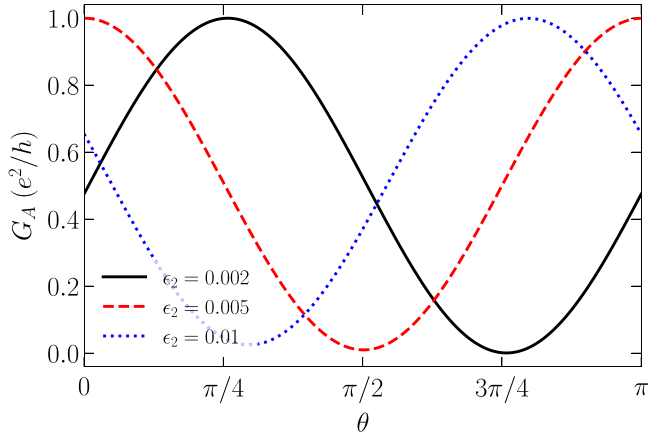
FIG. 14. The linear Andreev conductance G_A as a function of the spin canting angle θ obtained for $\varepsilon_1 = 0$, $V_M = 0.005$, $t = 0.01$, $\Gamma_S = 0.02$, $\Gamma_N = 0.002$, and several values of ε_2, as indicated.

APPENDIX B: MAJORANA SPECTRAL FUNCTIONS

For unambiguous identification of the Majorana modes leaking to each quantum dot in our geometry (Fig. 1), we have determined their spectral functions, following the procedure used in Refs. [10,18]. We represent $d_{i\sigma}^{(\dagger)}$ operators in the Majorana representation

$$\gamma_{i\sigma}^A = (d_{i\sigma}^\dagger + d_{i\sigma})/\sqrt{2}, \tag{B1}$$

$$\gamma_{i\sigma}^B = i(d_{i\sigma}^\dagger - d_{i\sigma})/\sqrt{2}. \tag{B2}$$

These Majorana operators are self-conjugate and satisfy the anticommutation rule $\{\gamma_{i\sigma}^\alpha, \gamma_{j\sigma'}^\beta\} = \delta_{\alpha,\beta}\delta_{i,j}\delta_{\sigma,\sigma'}$. In analogy to Eq. (11), we next introduce their spectral functions

$$\mathcal{M}_{i\sigma}^\alpha(\omega) = -\frac{1}{\pi}\text{Im}\langle\langle\gamma_{i\sigma}^\alpha;\gamma_{i\sigma}^\alpha\rangle\rangle_{\omega+i0^+}. \tag{B3}$$

For convenience we normalize them by the factor $\pi\Gamma_N$. Such dimensionless spectral functions $D_{i\sigma}^\alpha(\omega) = \pi\Gamma_N\mathcal{M}_{i\sigma}^\alpha(\omega)$ are formally related to the following spectral functions of each quantum dot in the initial representation [10]:

$$D_{i\sigma}^A(\omega) = -\frac{\Gamma_N}{2}\text{Im}(\langle\langle d_{i\sigma};d_{i\sigma}\rangle\rangle_{\omega+i0^+} + \langle\langle d_{i\sigma}^\dagger;d_{i\sigma}\rangle\rangle_{\omega+i0^+}$$
$$+ \langle\langle d_{i\sigma};d_{i\sigma}^\dagger\rangle\rangle_{\omega+i0^+} + \langle\langle d_{i\sigma}^\dagger;d_{i\sigma}^\dagger\rangle\rangle_{\omega+i0^+}) \tag{B4}$$

and

$$D_{i\sigma}^B(\omega) = -\frac{\Gamma_N}{2}\text{Im}(\langle\langle d_{i\sigma}^\dagger;d_{i\sigma}\rangle\rangle_{\omega+i0^+} + \langle\langle d_{i\sigma};d_{i\sigma}^\dagger\rangle\rangle_{\omega+i0^+}$$
$$- \langle\langle d_{i\sigma};d_{i\sigma}\rangle\rangle_{\omega+i0^+} - \langle\langle d_{i\sigma}^\dagger;d_{i\sigma}^\dagger\rangle\rangle_{\omega+i0^+}). \tag{B5}$$

Figures 15 and 16 display these spectral functions (B4) and (B5) obtained for the uncorrelated quantum dots with identical energy levels $\varepsilon_1 = \varepsilon_2 = 0$. We clearly notice that the zero-energy Majorana mode of A-type leaks to the neighboring QD$_2$ solely for spin-$\uparrow$, whereas to the outer QD$_1$ only in the spin-$\downarrow$ sector. Absence of the zero-energy quasiparticle of the opposite spin sectors is caused by the destructive interferometric effects, whose consequences observable in the charge tunneling are discussed in Sec. III C of this paper.

Upon detuning the energy levels $\varepsilon_1 \neq \varepsilon_2$, we observe signatures of the zero-energy Majorana A quasiparticle in
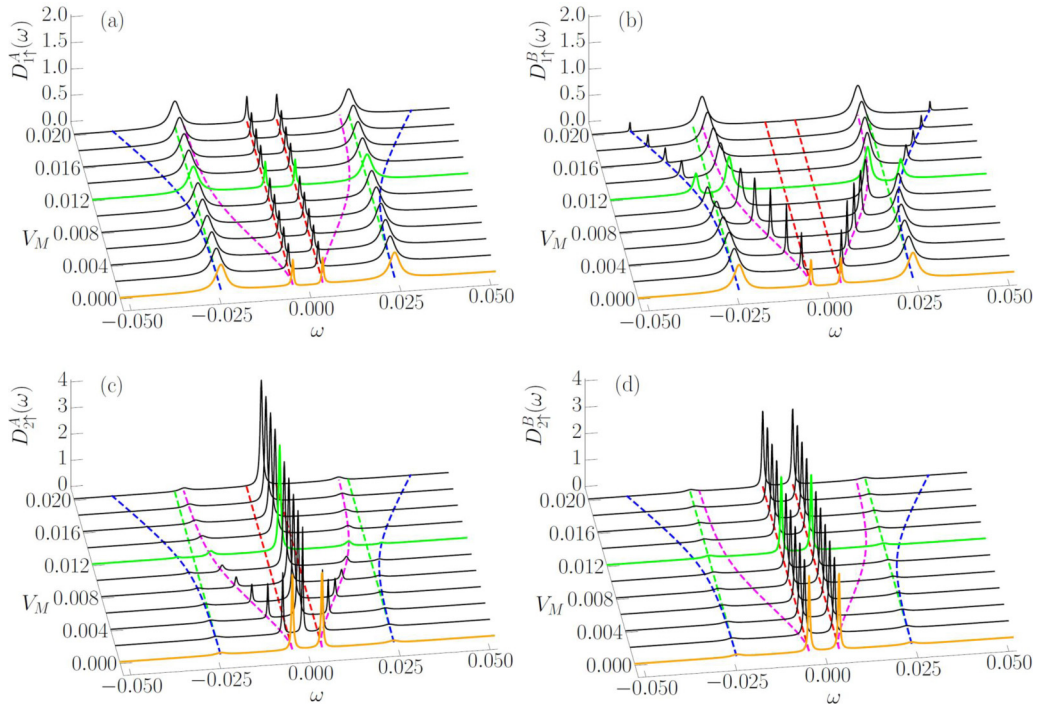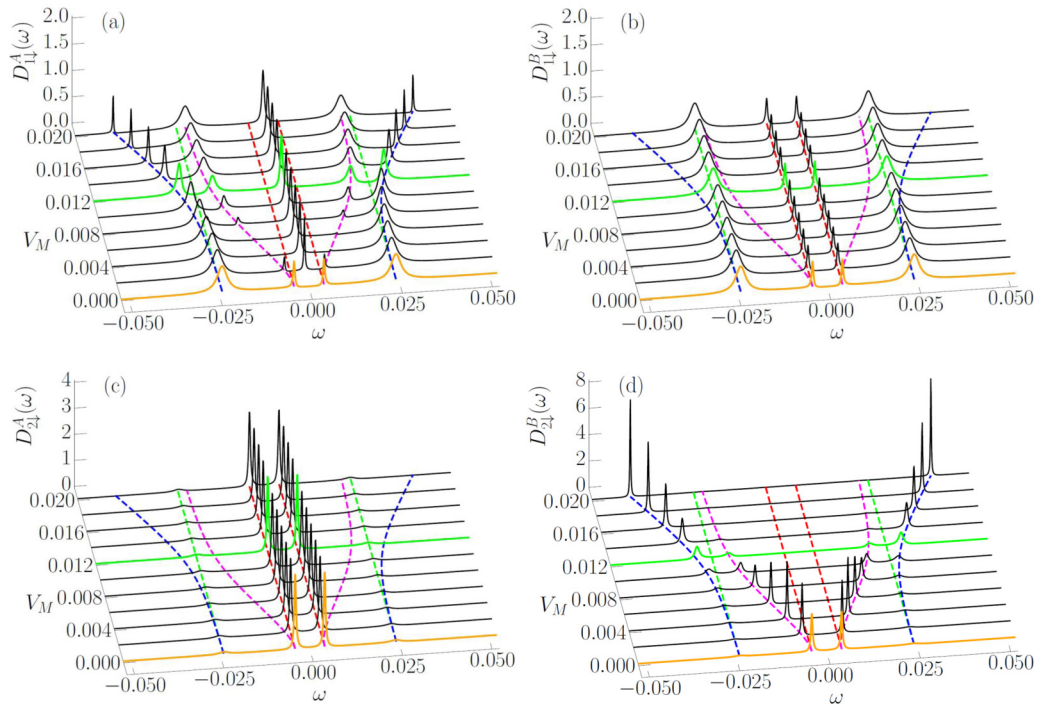

FIG. 15. The normalized Majorana spectral function $D_{i\uparrow}^\alpha$ induced at QD$_1$ (top) and QD$_2$ (bottom) for $\varepsilon_2 = 0$, using the model parameters presented in Fig. 2.

FIG. 16. The same as in Fig. 15 for spin ↓ electrons.

both spin sectors of each quantum dot, though with different magnitudes (due to partial interferometric effects). This behavior is shown in Figs. 17 and 18 for $\varepsilon_2 = 0.005$. The

tendency observed by us in this Appendix is reminiscent of the previous results displayed by Vernek *et al.* [18] in Fig. 2.
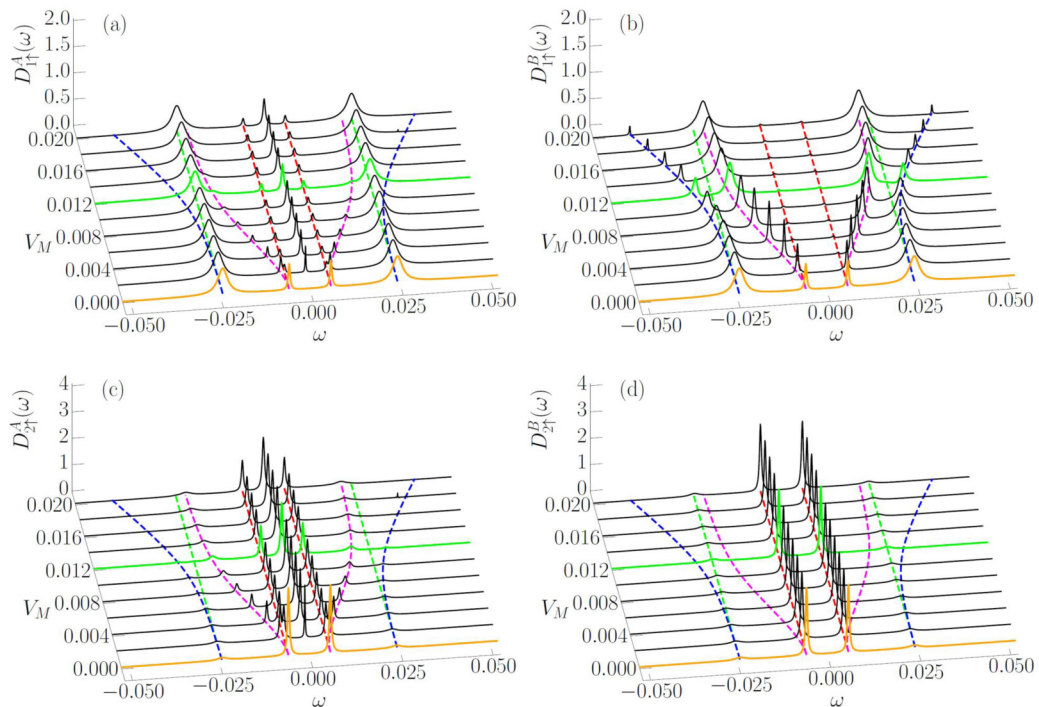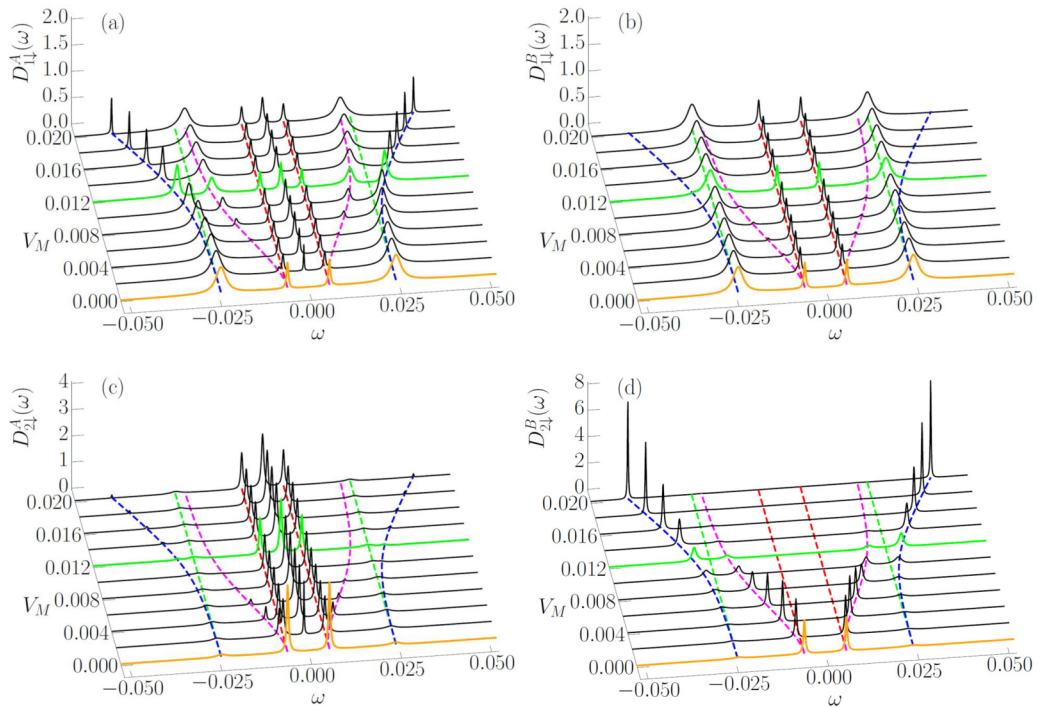

FIG. 17. The normalized Majorana spectral function $D_{i\uparrow}^\alpha$ induced at QD$_1$ (top) and QD$_2$ (bottom) for $\varepsilon_2 = 0.005$, using the model parameters presented in Fig. 2.

FIG. 18. The same as in Fig. 17 for spin ↓ electrons.

[1] W. G. van der Wiel, S. De Franceschi, J. M. Elzerman, T. Fujisawa, S. Tarucha, and L. P. Kouwenhoven, Electron transport through double quantum dots, Rev. Mod. Phys. **75**, 1 (2002).

[2] R. Hanson, L. P. Kouwenhoven, J. R. Petta, S. Tarucha, and L. M. K. Vandersypen, Spins in few-electron quantum dots, Rev. Mod. Phys. **79**, 1217 (2007).

[3] K. C. Nowack, F. H. L. Koppens, Y. V. Nazarov, and L. M. K. Vandersypen, Coherent control of a single electron spin with electric fields, Science **318**, 1430 (2007).

[4] A. Martín-Rodero and A. Levy Yeyati, Josephson and Andreev transport through quantum dots, Adv. Phys. **60**, 899 (2011).

[5] D. Sherman, J. S. Yodh, S. M. Albrecht, J. Nygård, P. Krogstrup, and C. M. Marcus, Normal, superconducting and topological regimes of hybrid double quantum dots, Nat. Nanotechnol. **12**, 212 (2017).

[6] T. W. Larsen, K. D. Petersson, F. Kuemmeth, T. S. Jespersen, P. Krogstrup, J. Nygård, and C. M. Marcus, Semiconductor-Nanowire-Based Superconducting Qubit, Phys. Rev. Lett. **115**, 127001 (2015).

[7] G. de Lange, B. van Heck, A. Bruno, D. J. van Woerkom, A. Geresdi, S. R. Plissard, E. P. A. M. Bakkers, A. R. Akhmerov, and L. DiCarlo, Realization of Microwave Quantum Circuits Using Hybrid Superconducting-Semiconducting Nanowire Josephson Elements, Phys. Rev. Lett. **115**, 127002 (2015).

[8] F. Luthi, T. Stavenga, O. W. Enzing, A. Bruno, C. Dickel, N. K. Langford, M. A. Rol, T. S. Jespersen, J. Nygård, P. Krogstrup, and L. DiCarlo, Evolution of Nanowire Transmon Qubits and Their Coherence in a Magnetic Field, Phys. Rev. Lett. **120**, 100502 (2018).

[9] M. Pita-Vidal, A. Bargerbos, C.-K. Yang, D. J. van Woerkom, W. Pfaff, N. Haider, P. Krogstrup, L. P. Kouwenhoven, G. de Lange, and A. Kou, Gate-Tunable Field-Compatible Fluxonium, Phys. Rev. Appl. **14**, 064038 (2020).

[10] J. F. Silva and E. Vernek, Andreev and Majorana bound states in single and double quantum dot structures, J. Phys.: Condens. Matter **28**, 435702 (2016).

[11] T. I. Ivanov, Coherent tunneling through a double quantum dot coupled to Majorana bound states, Phys. Rev. B **96**, 035417 (2017).

[12] Z. Su, A. B. Tacla, M. Hocevar, D. Car, S. R. Plissard, E. P. A. M. Bakkers, A. J. Daley, D. Pekker, and S. M. Frolov, Andreev molecules in semiconductor nanowire double quantum dots, Nat. Commun. **8**, 585 (2017).

[13] M. J. Rančić, S. Hoffman, C. Schrade, J. Klinovaja, and D. Loss, Entangling spins in double quantum dots and Majorana bound states, Phys. Rev. B **99**, 165306 (2019).

[14] J. D. Cifuentes and L. G. G. V. D. da Silva, Manipulating Majorana zero modes in double quantum dots, Phys. Rev. B **100**, 085429 (2019).

[15] I. Weymann, K. P. Wójcik, and P. Majek, Majorana-Kondo interplay in T-shaped double quantum dots, Phys. Rev. B **101**, 235404 (2020).

[16] D. Aasen, M. Hell, R. V. Mishmash, A. Higginbotham, J. Danon, M. Leijnse, T. S. Jespersen, J. A. Folk, C. M. Marcus, K. Flensberg, and J. Alicea, Milestones Toward Majorana-Based Quantum Computing Phys. Rev. X, **6**, 031016 (2016).

[17] M. T. Deng, S. Vaitiekenas, E. B. Hansen, J. Danon, M. Leijnse, K. Flensberg, J. Nygård, P. Krogstrup, and C. M. Marcus, Majorana bound state in a coupled quantum-dot hybrid-nanowire system, Science **354**, 1557 (2016).

[18] E. Vernek, P. H. Penteado, A. C. Seridonio, and J. C. Egues, Subtle leakage of a Majorana mode into a quantum dot, Phys. Rev. B **89**, 165314 (2014).

[19] E. Prada, P. San-Jose, M. W. A. de Moor, A. Geresdi, E. J. H. Lee, J. Klinovaja, D. Loss, J. Nygård, R. Aguado, and L. P. Kouwenhoven, From Andreev to Majorana bound states in hybrid superconductor-semiconductor nanowires, Nat. Rev. Phys. **2**, 575 (2020).

[20] M. Lee, J. S. Lim, and R. López, Kondo effect in a quantum dot side-coupled to a topological superconductor, Phys. Rev. B **87**, 241402(R) (2013).

[21] M. Cheng, M. Becker, B. Bauer, and R. M. Lutchyn, Interplay between Kondo and Majorana Interactions in Quantum Dots, Phys. Rev. X **4**, 031051 (2014).

[22] D. A. Ruiz-Tijerina, E. Vernek, L. G. G. V. D. da Silva, and J. C. Egues, Interaction effects on a Majorana zero mode leaking into a quantum dot, Phys. Rev. B **91**, 115435(R) (2015).

[23] I. Weymann, Spin Seebeck effect in quantum dot side-coupled to topological superconductor, J. Phys.: Condens. Matter **29**, 095301 (2017).

[24] I. Weymann and K. P. Wójcik, Transport properties of a hybrid Majorana wire-quantum dot system with ferromagnetic contacts, Phys. Rev. B **95**, 155427 (2017).

[25] M.-T. Deng, S. Vaitiekėnas, E. Prada, P. San-Jose, J. Nygård, P. Krogstrup, R. Aguado, and C. M. Marcus, Nonlocality of Majorana modes in hybrid nanowires, Phys. Rev. B **98**, 085125 (2018).

[26] G. Górski, J. Barański, I. Weymann, and T. Domański, Interplay between correlations and Majorana mode in proximitized quantum dot, Sci. Rep. **8**, 15717 (2018).

[27] J. F. Silva, L. G. G. V. Dias da Silva, and E. Vernek, Robustness of the Kondo effect in a quantum dot coupled to Majorana zero modes, Phys. Rev. B **101**, 075428 (2020).

[28] P. Majek, K. P. Wójcik, and I. Weymann, Spin-resolved thermal signatures of Majorana-Kondo interplay in double quantum dots, Phys. Rev. B **105**, 075418 (2022).

[29] K. Grove-Rasmussen, G. Steffensen, A. Jellinggaard, M. H. Madsen, R. Žitko, J. Paaske, and J. Nygård, Yu-Shiba-Rusinov screening of spins in double quantum dots, Nat. Commun. **9**, 2376 (2018).

[30] J. C. Estrada Saldaña, A. Vekris, G. Steffensen, R. Žitko, P. Krogstrup, J. Paaske, K. Grove-Rasmussen, and J. Nygård, Supercurrent in a Double Quantum Dot, Phys. Rev. Lett. **121**, 257701 (2018).

[31] D. Bouman, R. J. J. van Gulik, G. Steffensen, D. Pataki, P. Boross, P. Krogstrup, J. Nygård, J. Paaske, A. Pályi, and A. Geresdi, Triplet-blockaded Josephson supercurrent in double quantum dots, Phys. Rev. B **102**, 220505(R) (2020).

[32] J. C. Estrada Saldaña, A. Vekris, R. Žitko, G. Steffensen, P. Krogstrup, J. Paaske, K. Grove-Rasmussen, and J. Nygård, Two-impurity Yu-Shiba-Rusinov states in coupled quantum dots, Phys. Rev. B **102**, 195143 (2020).

[33] A. Zarassi, Z. Su, J. Danon, J. Schwenderling, M. Hocevar, B. M. Nguyen, J. Yoo, S. A. Dayeh, and S. M. Frolov, Magnetic field evolution of spin blockade in Ge/Si nanowire double quantum dots, Phys. Rev. B **95**, 155416 (2017).

[34] J.-P. Cleuziou, W. Wernsdorfer, V. Bouchiat, T. Ondarcuhu, and M. Monthioux, Carbon nanotube superconducting quantum interference device, Nat. Nanotechnol. **1**, 53 (2006).

[35] J.-D. Pillet, P. Joyez, R. Žitko, and M. F. Goffman, Tunneling spectroscopy of a single quantum dot coupled to a superconductor: From Kondo ridge to Andreev bound states, Phys. Rev. B **88**, 045101 (2013).

[36] M. Ruby, B. W. Heinrich, Y. Peng, F. von Oppen, and K. J. Franke, Wave-Function Hybridization in Yu-Shiba-Rusinov Dimers, Phys. Rev. Lett. **120**, 156803 (2018).

[37] B. W. Heinrich, J. I. Pascual, and K. J. Franke, Single magnetic adsorbates on *s*-wave superconductors, Prog. Surf. Sci. **93**, 1 (2018).

[38] D.-J. Choi, C. G. Fernández, E. Herrera, C. Rubio-Verdú, M. M. Ugeda, I. Guillamón, H. Suderow, J. I. Pascual, and N. Lorente, Influence of magnetic ordering between Cr adatoms on the Yu-Shiba-Rusinov States of the β-Bi$_2$Pd Superconductor, Phys. Rev. Lett. **120**, 167001 (2018).

[39] S. Kezilebieke, R. Žitko, M. Dvorak, and P. Liljeroth, Observation of coexistence of Yu-Shiba-Rusinov states and spin-flip excitations, Nano Lett. **19**, 4614 (2019).

[40] M.-S. Choi, C. Bruder, and D. Loss, Spin-dependent Josephson current through double quantum dots and measurement of entangled electron states, Phys. Rev. B **62**, 13569 (2000).

[41] Y. Zhu, Q.-F. Sun, and T.-H. Lin, Probing spin states of coupled quantum dots by a dc Josephson current, Phys. Rev. B **66**, 085306 (2002).

[42] Y. Tanaka, N. Kawakami, and A. Oguri, Correlated electron transport through double quantum dots coupled to normal and superconducting leads, Phys. Rev. B **81**, 075404 (2010).

[43] R. Žitko, M. Lee, R. López, R. Aguado, and M.-S. Choi, Josephson Current in Strongly Correlated Double Quantum Dots, Phys. Rev. Lett. **105**, 116803 (2010).

[44] J. Eldridge, M. G. Pala, M. Governale, and J. König, Superconducting proximity effect in interacting double-dot systems, Phys. Rev. B **82**, 184507 (2010).

[45] S. Droste, S. Andergassen, and J. Splettstoesser, Josephson current through interacting double quantum dots with spin–orbit coupling, J. Phys.: Condens. Matter **24**, 415301 (2012).

[46] S. Pfaller, A. Donarini, and M. Grifoni, Subgap features due to quasiparticle tunneling in quantum dots coupled to superconducting leads, Phys. Rev. B **87**, 155439 (2013).

[47] B. Sothmann, S. Weiss, M. Governale, and J. König, Unconventional superconductivity in double quantum dots, Phys. Rev. B **90**, 220501(R) (2014).

[48] N. Y. Yao, C. P. Moca, I. Weymann, J. D. Sau, M. D. Lukin, E. A. Demler, and G. Zaránd, Phase diagram and excitations of a Shiba molecule, Phys. Rev. B **90**, 241108(R) (2014).

[49] T. Meng, J. Klinovaja, S. Hoffman, P. Simon, and D. Loss, Superconducting gap renormalization around two magnetic impurities: From Shiba to Andreev bound states, Phys. Rev. B **92**, 064503 (2015).

[50] R. Žitko, Numerical subgap spectroscopy of double quantum dots coupled to superconductors, Phys. Rev. B **91**, 165116 (2015).

[51] K. Wrześniewski and I. Weymann, Kondo physics in double quantum dot based Cooper pair splitters, Phys. Rev. B **96**, 195409 (2017).

[52] A. Ptok, S. Głodzik, and T. Domański, Yu-Shiba-Rusinov states of impurities in a triangular lattice of NbSe$_2$ with spin-orbit coupling, Phys. Rev. B **96**, 184425 (2017).

[53] D. Pekker, P. Zhang, and S. M. Frolov, Theory of Andreev blockade in a double quantum dot with a superconducting lead, SciPost Phys. **11**, 081 (2021).

[54] Z. Scherübl, A. Pályi, and S. Csonka, Transport signatures of an Andreev molecule in a quantum dot-superconductor-quantum dot setup, Beilstein J. Nanotechnol. **10**, 363 (2019).

[55] V. Pokorný, M. Žonda, G. Loukeris, and T Novotný, Second order perturbation theory for a superconducting double quantum dot, JPS Conf. Proc. **30**, 011002 (2020).

[56] X.-Q. Wang, S.-F. Zhang, Y. Han, and W.-J. Gong, Fano-Andreev effect in a parallel double quantum dot structure, Phys. Rev. B **100**, 115405 (2019).

[57] Z.-Z. Li and M. Leijnse, Quantum interference in transport through almost symmetric double quantum dots, Phys. Rev. B **99**, 125406 (2019).

[58] D. K. Morr and N. A. Stavropoulos, Quantum interference between impurities: Creating novel many-body states in *s*-wave superconductors, Phys. Rev. B **67**, 020502(R) (2003).

[59] D. K. Morr and J. Yoon, Impurities, quantum interference, and quantum phase transitions in *s*-wave superconductors, Phys. Rev. B **73**, 224511 (2006).

[60] A. Brunetti, A. Zazunov, A. Kundu, and R. Egger, Anomalous Josephson current, incipient time-reversal symmetry breaking, and Majorana bound states in interacting multilevel dots, Phys. Rev. B **88**, 144515 (2013).

[61] C. Jünger, S. Lehmann, K. A. Dick, C. Thelander, C. Schönenberger, and A. Baumgartner, Intermediate states in Andreev bound state fusion, arXiv:2111.00651.

[62] K. Flensberg, F. von Oppen, and A. Stern, Engineered platforms for topological superconductivity and Majorana zero modes, arXiv:2103.05548.

[63] K. G. Wilson, The renormalization group: Critical phenomena and the Kondo problem, Rev. Mod. Phys. **47**, 773 (1975).

[64] A. Weichselbaum and J. von Delft, Sum-Rule Conserving Spectral Functions from the Numerical Renormalization Group, Phys. Rev. Lett. **99**, 076402 (2007).

[65] R. Bulla, T. A. Costi, and T. Pruschke, Numerical renormalization group method for quantum impurity systems, Rev. Mod. Phys. **80**, 395 (2008).

[66] A. I. Tóth, C. P. Moca, Ö. Legeza, and G. Zaránd, Density matrix numerical renormalization group for non-Abelian symmetries, Phys. Rev. B **78**, 245109 (2008).

[67] Ö. Legeza, C. P. Moca, A. I. Tóth, I. Weymann, and G. Zaránd, Manual for the Flexible DM-NRG code, arXiv:0809.3143; the open access Flexible DM-NRG Budapest code is available at http://www.phy.bme.hu/~dmnrg/.

[68] S. Hoffman, D. Chevallier, D. Loss, and J. Klinovaja, Spin-dependent coupling between quantum dots and topological quantum wires, Phys. Rev. B **96**, 045440(R) (2017).

[69] E. Prada, R. Aguado, and P. San-Jose, Measuring Majorana nonlocality and spin structure with a quantum dot, Phys. Rev. B **96**, 085418 (2017).

[70] A. Schuray, A. L. Yeyati, and P. Recher, Influence of the Majorana nonlocality on the supercurrent, Phys. Rev. B **98**, 235301 (2018).

[71] D. E. Liu and H. U. Baranger, Detecting a Majorana-fermion zero mode using a quantum dot, Phys. Rev. B **84**, 201308(R) (2011).

[72] M. Leijnse and K. Flensberg, Scheme to measure Majorana fermion lifetimes using a quantum dot, Phys. Rev. B **84**, 140501(R) (2011).

[73] G. Górski and K. Kucab, Transport properties of proximitized double quantum dots, Physica E **126**, 114459 (2021).

[74] Y. Tanaka, N. Kawakami, and A. Oguri, Andreev transport through side-coupled double quantum dots, Phys. Rev. B **78**, 035444 (2008).

[75] J. Barański and T. Domański, Fano-type interference in quantum dots coupled between metallic and superconducting leads, Phys. Rev. B **84**, 195424 (2011).

[76] J. Barański and T. Domański, Decoherence effect on Fano line shapes in double quantum dots coupled between normal and superconducting leads, Phys. Rev. B **85**, 205451 (2012).

[77] J. Barański, T. Zienkiewicz, M. Barańska, and K. J. Kapcia, Anomalous Fano resonance in double quantum dot system coupled to superconductor, Sci. Rep. **10**, 2881 (2020).

[78] M. T. Deng, C. L. Yu, G. Y. Huang, M. Larsson, P. Caroff, and H. Q. Xu, Anomalous zero-bias conductance peak in a Nb-InSb nanowire-Nb hybrid device, Nano Lett. **12**, 6414 (2012).

[79] V. Mourik, K. Zuo, S. M. Frolov, S. R. Plissard, E. P. A. M. Bakkers, and L. P. Kouwenhoven, Signatures of Majorana fermions in hybrid superconductor-semiconductor nanowire devices, Science **336**, 1003 (2012).

[80] A. Das, Y. Ronen, Y. Most, Y. Oreg, M. Heiblum, and H. Shtrikman, Zero-bias peaks and splitting in an al-inas nanowire topological superconductor as a signature of Majorana fermions, Nat. Phys. **8**, 887 (2012).

[81] H. O. H. Churchill, V. Fatemi, K. Grove-Rasmussen, M. T. Deng, P. Caroff, H. Q. Xu, and C. M. Marcus, Superconductor-nanowire devices from tunneling to the multichannel regime: Zero-bias oscillations and magnetoconductance crossover, Phys. Rev. B **87**, 241401(R) (2013).

[82] R. S. Deacon, Y. Tanaka, A. Oiwa, R. Sakano, K. Yoshida, K. Shibata, K. Hirakawa, and S. Tarucha, Kondo-enhanced Andreev transport in single self-assembled InAs quantum dots contacted with normal and superconducting leads, Phys. Rev. B **81**, 121308(R) (2010).

[83] R. S. Deacon, Y. Tanaka, A. Oiwa, R. Sakano, K. Yoshida, K. Shibata, K. Hirakawa, and S. Tarucha, Tunneling Spectroscopy of Andreev Energy Levels in a Quantum Dot Coupled to a Superconductor, Phys. Rev. Lett. **104**, 076805 (2010).

[84] F. Hübler, M. J. Wolf, T. Scherer, D. Wang, D. Beckmann, and H. v. Löhneysen, Observation of Andreev Bound States at Spin-Active Interfaces, Phys. Rev. Lett. **109**, 087004 (2012).

[85] W. Chang, V. E. Manucharyan, T. S. Jespersen, J. Nygård, and C. M. Marcus, Tunneling Spectroscopy of Quasiparticle Bound States in a Spinful Josephson Junction, Phys. Rev. Lett. **110**, 217005 (2013).

[86] M. R. Buitelaar, T. Nussbaumer, and C. Schönenberger, Quantum Dot in the Kondo Regime Coupled to Superconductors, Phys. Rev. Lett. **89**, 256801 (2002).

[87] V. Koerting, B. M. Andersen, K. Flensberg, and J. Paaske, Nonequilibrium transport via spin-induced subgap states in superconductor/quantum dot/normal metal cotunnel junctions, Phys. Rev. B **82**, 245108 (2010).

[88] J. Barański and T. Domański, In-gap states of a quantum dot coupled between a normal and a superconducting lead, J. Phys.: Condens. Matter **25**, 435305 (2013).

[89] J. Barański, A. Kobiałka, and T. Domański, Spin-sensitive interference due to Majorana state on the interface between normal and superconducting leads, J. Phys.: Condens. Matter **29**, 075603 (2017).

[90] T. Zienkiewicz, J. Barański, G. Górski, and T. Domański, Leakage of Majorana mode into correlated quantum dot nearby its singlet-doublet crossover, J. Phys.: Condens. Matter **32**, 025302 (2020).

[91] J. Kondo, Resistance minimum in dilute magnetic alloys, Prog. Theor. Phys. **32**, 37 (1964).

[92] A. C. Hewson, *The Kondo Problem to Heavy Fermions* (Cambridge University Press, Cambridge, UK, 1993).

[93] J. Bauer, A. Oguri, and A. C. Hewson, Spectral properties of locally correlated electrons in a Bardeen-Cooper-Schrieffer superconductor, J. Phys.: Condens. Matter **19**, 486211 (2007).

[94] R. Žitko, J. S. Lim, R. López, and R. Aguado, Shiba states and zero-bias anomalies in the hybrid normal-superconductor Anderson model, Phys. Rev. B **91**, 045441 (2015).

[95] T. Domański, I. Weymann, M. Barańska, and G. Górski, Constructive influence of the induced electron pairing on the Kondo state, Sci. Rep. **6**, 23336 (2016).

[96] K. P. Wójcik and I. Weymann, Nonlocal pairing as a source of spin exchange and Kondo screening, Phys. Rev. B **99**, 045120 (2019).

[97] P. Majek and I. Weymann, Majorana mode leaking into a spin-charge entangled double quantum dot, Phys. Rev. B **104**, 085416 (2021).

[98] D. Goldhaber-Gordon, H. Shtrikman, D. Mahalu, D. Abusch-Magder, U. Meirav, and M. A. Kastner, Kondo effect in a single-electron transistor, Nature (London) **391**, 156 (1998).

[99] M. Pustilnik and L. I. Glazman, Kondo Effect in Real Quantum Dots, Phys. Rev. Lett. **87**, 216601 (2001).

[100] P. S. Cornaglia and D. R. Grempel, Strongly correlated regimes in a double quantum dot device, Phys. Rev. B **71**, 075305 (2005).

[101] C.-H. Chung, G. Zarand, and P. Wölfle, Two-stage Kondo effect in side-coupled quantum dots: Renormalized perturbative scaling theory and numerical renormalization group analysis, Phys. Rev. B **77**, 035120 (2008).

[102] K. P. Wójcik and I. Weymann, Two-stage Kondo effect in T-shaped double quantum dots with ferromagnetic leads, Phys. Rev. B **91**, 134422 (2015).

[103] A. Calzona and B. Trauzettel, Spin-resolved spectroscopy of helical Andreev bound states, Phys. Rev. Res. **4**, 013182 (2022).

[104] G. S. Diniz and E. Vernek, Majorana correlations in quantum impurities coupled to a topological wire, arXiv:2208.09524.